

1 A Statistical Approach to Recognizing Source Classes for Unassociated Sources 2 in the First Fermi-LAT Catalog

3 M. Ackermann², M. Ajello³, A. Allafort³, E. Antolini^{4,5}, L. Baldini⁶, J. Ballet⁷, G. Barbiellini^{8,9},
4 D. Bastieri^{10,11}, R. Bellazzini⁶, B. Berenji³, R. D. Blandford³, E. D. Bloom³, E. Bonamente^{4,5},
5 A. W. Borgland³, A. Bouvier¹², T. J. Brandt^{13,14}, J. Bregeon⁶, M. Brigida^{15,16}, P. Bruel¹⁷,
6 R. Buehler³, T. H. Burnett¹⁸, S. Buson^{10,11}, G. A. Caliandro¹⁹, R. A. Cameron³, P. A. Caraveo²⁰,
7 J. M. Casandjian⁷, E. Cavazzuti²¹, C. Cecchi^{4,5}, Ö. Çelik^{22,23,24}, E. Charles³, A. Chekhtman²⁵,
8 A. W. Chen²⁰, C. C. Cheung²⁶, J. Chiang³, S. Ciprini^{27,5}, R. Claus³, J. Cohen-Tanugi²⁸,
9 J. Conrad^{29,30,31}, S. Cutini²¹, A. de Angelis³², M. E. DeCesar^{22,33}, A. De Luca³⁴,
10 F. de Palma^{15,16}, C. D. Dermer³⁵, E. do Couto e Silva³, P. S. Drell³, A. Drlica-Wagner³,
11 R. Dubois³, T. Enoto³, C. Favuzzi^{15,16}, S. J. Fegan¹⁷, E. C. Ferrara^{22,1}, W. B. Focke³, P. Fortin¹⁷,
12 Y. Fukazawa³⁶, S. Funk³, P. Fusco^{15,16}, F. Gargano¹⁶, D. Gasparrini²¹, N. Gehrels²²,
13 S. Germani^{4,5}, N. Giglietto^{15,16}, F. Giordano^{15,16}, M. Giroletti³⁷, T. Glanzman³, G. Godfrey³,
14 I. A. Grenier⁷, M.-H. Grondin^{38,39}, J. E. Grove³⁵, L. Guillemot⁴⁰, S. Guiriec⁴¹, M. Gustafsson¹⁰,
15 D. Hadasch¹⁹, Y. Hanabata³⁶, A. K. Harding²², M. Hayashida^{3,42}, E. Hays²², S. E. Healey³,
16 A. B. Hill⁴³, D. Horan¹⁷, X. Hou⁴⁴, G. Jóhannesson⁴⁵, A. S. Johnson³, T. J. Johnson²⁶,
17 T. Kamae³, H. Katagiri⁴⁶, J. Kataoka⁴⁷, M. Kerr³, J. Knödseder^{13,14}, M. Kuss⁶, J. Lande³,
18 L. Latronico⁴⁸, S.-H. Lee⁴⁹, M. Lemoine-Goumard^{50,51}, F. Longo^{8,9}, F. Loparco^{15,16}, B. Lott⁵⁰,
19 M. N. Lovellette³⁵, P. Lubrano^{4,5}, G. M. Madejski³, M. N. Mazziotta¹⁶, J. E. McEnery^{22,33},
20 J. Mehalt²⁸, P. F. Michelson³, R. P. Mignani⁵², W. Mitthumsiri³, T. Mizuno³⁶, C. Monte^{15,16},
21 M. E. Monzani^{3,1}, A. Morselli⁵³, I. V. Moskalenko³, S. Murgia³, T. Nakamori⁴⁷,
22 M. Naumann-Godo⁷, P. L. Nolan^{3,54}, J. P. Norris⁵⁵, E. Nuss²⁸, T. Ohsugi⁵⁶, A. Okumura^{3,57},
23 N. Omodei³, E. Orlando^{3,58}, J. F. Ormes⁵⁹, M. Ozaki⁵⁷, D. Paneque^{60,3}, J. H. Panetta³,
24 D. Parent⁶¹, V. Pelassa⁴¹, M. Pesce-Rollins⁶, M. Pierbattista⁷, F. Piron²⁸, G. Pivato¹¹,
25 T. A. Porter^{3,3}, S. Rainò^{15,16}, R. Rando^{10,11}, P. S. Ray³⁵, M. Razzano^{6,12}, A. Reimer^{62,3},
26 O. Reimer^{62,3}, T. Reposeur⁵⁰, R. W. Romani³, H. F.-W. Sadrozinski¹², D. Salvetti^{20,1},
27 P. M. Saz Parkinson¹², T. L. Schalk¹², C. Sgrò⁶, M. S. Shaw³, E. J. Siskind⁶³, P. D. Smith⁶⁴,
28 G. Spandre⁶, P. Spinelli^{15,16}, D. J. Suson⁶⁵, H. Takahashi⁵⁶, T. Tanaka³, J. G. Thayer³,
29 J. B. Thayer³, D. J. Thompson²², L. Tibaldo^{10,11}, O. Tibolla⁶⁶, D. F. Torres^{19,67}, G. Tosti^{4,5},
30 A. Tramacere^{3,68,69}, E. Troja^{22,70}, T. L. Usher³, J. Vandenbroucke³, V. Vasileiou²⁸,
31 G. Vianello^{3,68}, N. Vilchez^{13,14,1}, V. Vitale^{53,71}, A. P. Waite³, E. Wallace¹⁸, P. Wang³,
32 B. L. Winer⁶⁴, M. T. Wolff³⁵, D. L. Wood⁷², K. S. Wood³⁵, Z. Yang^{29,30}, S. Zimmer^{29,30}

¹Corresponding authors: E. C. Ferrara, elizabeth.c.ferrara@nasa.gov; M. E. Monzani, monzani@slac.stanford.edu; D. Salvetti, salvetti@lambrate.inaf.it; N. Vilchez, vilchez@cesr.fr.

²Deutsches Elektronen Synchrotron DESY, D-15738 Zeuthen, Germany

³W. W. Hansen Experimental Physics Laboratory, Kavli Institute for Particle Astrophysics and Cosmology, Department of Physics and SLAC National Accelerator Laboratory, Stanford University, Stanford, CA 94305, USA

⁴Istituto Nazionale di Fisica Nucleare, Sezione di Perugia, I-06123 Perugia, Italy

⁵Dipartimento di Fisica, Università degli Studi di Perugia, I-06123 Perugia, Italy

⁶Istituto Nazionale di Fisica Nucleare, Sezione di Pisa, I-56127 Pisa, Italy

⁷Laboratoire AIM, CEA-IRFU/CNRS/Université Paris Diderot, Service d’Astrophysique, CEA Saclay, 91191 Gif sur Yvette, France

⁸Istituto Nazionale di Fisica Nucleare, Sezione di Trieste, I-34127 Trieste, Italy

⁹Dipartimento di Fisica, Università di Trieste, I-34127 Trieste, Italy

¹⁰Istituto Nazionale di Fisica Nucleare, Sezione di Padova, I-35131 Padova, Italy

¹¹Dipartimento di Fisica “G. Galilei”, Università di Padova, I-35131 Padova, Italy

¹²Santa Cruz Institute for Particle Physics, Department of Physics and Department of Astronomy and Astrophysics, University of California at Santa Cruz, Santa Cruz, CA 95064, USA

¹³CNRS, IRAP, F-31028 Toulouse cedex 4, France

¹⁴GAHEC, Université de Toulouse, UPS-OMP, IRAP, Toulouse, France

¹⁵Dipartimento di Fisica “M. Merlin” dell’Università e del Politecnico di Bari, I-70126 Bari, Italy

¹⁶Istituto Nazionale di Fisica Nucleare, Sezione di Bari, 70126 Bari, Italy

¹⁷Laboratoire Leprince-Ringuet, École polytechnique, CNRS/IN2P3, Palaiseau, France

¹⁸Department of Physics, University of Washington, Seattle, WA 98195-1560, USA

¹⁹Institut de Ciències de l’Espai (IEEE-CSIC), Campus UAB, 08193 Barcelona, Spain

²⁰INAF-Istituto di Astrofisica Spaziale e Fisica Cosmica, I-20133 Milano, Italy

²¹Agenzia Spaziale Italiana (ASI) Science Data Center, I-00044 Frascati (Roma), Italy

²²NASA Goddard Space Flight Center, Greenbelt, MD 20771, USA

²³Center for Research and Exploration in Space Science and Technology (CRESST) and NASA Goddard Space Flight Center, Greenbelt, MD 20771, USA

²⁴Department of Physics and Center for Space Sciences and Technology, University of Maryland Baltimore County, Baltimore, MD 21250, USA

²⁵Artep Inc., 2922 Excelsior Springs Court, Ellicott City, MD 21042, resident at Naval Research Laboratory, Washington, DC 20375, USA

²⁶National Research Council Research Associate, National Academy of Sciences, Washington, DC 20001, resident at Naval Research Laboratory, Washington, DC 20375, USA

²⁷ASI Science Data Center, I-00044 Frascati (Roma), Italy

²⁸Laboratoire Univers et Particules de Montpellier, Université Montpellier 2, CNRS/IN2P3, Montpellier, France

-
- ²⁹Department of Physics, Stockholm University, AlbaNova, SE-106 91 Stockholm, Sweden
- ³⁰The Oskar Klein Centre for Cosmoparticle Physics, AlbaNova, SE-106 91 Stockholm, Sweden
- ³¹Royal Swedish Academy of Sciences Research Fellow, funded by a grant from the K. A. Wallenberg Foundation
- ³²Dipartimento di Fisica, Università di Udine and Istituto Nazionale di Fisica Nucleare, Sezione di Trieste, Gruppo Collegato di Udine, I-33100 Udine, Italy
- ³³Department of Physics and Department of Astronomy, University of Maryland, College Park, MD 20742, USA
- ³⁴Istituto Universitario di Studi Superiori (IUSS), I-27100 Pavia, Italy
- ³⁵Space Science Division, Naval Research Laboratory, Washington, DC 20375-5352, USA
- ³⁶Department of Physical Sciences, Hiroshima University, Higashi-Hiroshima, Hiroshima 739-8526, Japan
- ³⁷INAF Istituto di Radioastronomia, 40129 Bologna, Italy
- ³⁸Max-Planck-Institut für Kernphysik, D-69029 Heidelberg, Germany
- ³⁹Landessternwarte, Universität Heidelberg, Königstuhl, D 69117 Heidelberg, Germany
- ⁴⁰Max-Planck-Institut für Radioastronomie, Auf dem Hügel 69, 53121 Bonn, Germany
- ⁴¹Center for Space Plasma and Aeronomic Research (CSPAR), University of Alabama in Huntsville, Huntsville, AL 35899, USA
- ⁴²Department of Astronomy, Graduate School of Science, Kyoto University, Sakyo-ku, Kyoto 606-8502, Japan
- ⁴³School of Physics and Astronomy, University of Southampton, Highfield, Southampton, SO17 1BJ, UK
- ⁴⁴Centre d'Études Nucléaires de Bordeaux Gradignan, IN2P3/CNRS, Université Bordeaux 1, BP120, F-33175 Gradignan Cedex, France
- ⁴⁵Science Institute, University of Iceland, IS-107 Reykjavik, Iceland
- ⁴⁶College of Science, Ibaraki University, 2-1-1, Bunkyo, Mito 310-8512, Japan
- ⁴⁷Research Institute for Science and Engineering, Waseda University, 3-4-1, Okubo, Shinjuku, Tokyo 169-8555, Japan
- ⁴⁸Istituto Nazionale di Fisica Nucleare, Sezione di Torino, I-10125 Torino, Italy
- ⁴⁹Yukawa Institute for Theoretical Physics, Kyoto University, Kitashirakawa Oiwake-cho, Sakyo-ku, Kyoto 606-8502, Japan
- ⁵⁰Université Bordeaux 1, CNRS/IN2p3, Centre d'Études Nucléaires de Bordeaux Gradignan, 33175 Gradignan, France
- ⁵¹Funded by contract ERC-StG-259391 from the European Community
- ⁵²Mullard Space Science Laboratory, University College London, Holmbury St. Mary, Dorking, Surrey, RH5 6NT, UK
- ⁵³Istituto Nazionale di Fisica Nucleare, Sezione di Roma “Tor Vergata”, I-00133 Roma, Italy
- ⁵⁴Deceased
- ⁵⁵Department of Physics, Boise State University, Boise, ID 83725, USA
- ⁵⁶Hiroshima Astrophysical Science Center, Hiroshima University, Higashi-Hiroshima, Hiroshima 739-8526, Japan

ABSTRACT

33

34

The *Fermi* Large Area Telescope First Source Catalog (1FGL) provided spatial, spectral, and temporal properties for a large number of γ -ray sources using a uniform analysis method. After correlating with the most-complete catalogs of source types known to emit γ rays, 630 of these sources are “unassociated” (i.e. have no obvious counterparts at other wavelengths). Here, we employ two statistical analyses of the primary γ -ray characteristics for these unassociated sources in an effort to correlate their γ -ray properties with the AGN and pulsar populations in 1FGL. Based on the correlation results, we classify 221 AGN-like and 134 pulsar-like sources in the 1FGL unassociated sources. The results of these source “classifications” appear to match the expected source distributions, especially at high Galactic latitudes. While useful for planning future multiwavelength follow-up observations, these analyses use limited inputs, and their predictions should not be considered equivalent to “probable source classes” for these sources. We discuss multiwavelength results and catalog cross-correlations to date, and provide new source associations for 229 *Fermi*-LAT sources that had no association listed in the 1FGL catalog. By validating the source classifications against these new

⁵⁷Institute of Space and Astronautical Science, JAXA, 3-1-1 Yoshinodai, Chuo-ku, Sagami-hara, Kanagawa 252-5210, Japan

⁵⁸Max-Planck Institut für extraterrestrische Physik, 85748 Garching, Germany

⁵⁹Department of Physics and Astronomy, University of Denver, Denver, CO 80208, USA

⁶⁰Max-Planck-Institut für Physik, D-80805 München, Germany

⁶¹Center for Earth Observing and Space Research, College of Science, George Mason University, Fairfax, VA 22030, resident at Naval Research Laboratory, Washington, DC 20375, USA

⁶²Institut für Astro- und Teilchenphysik and Institut für Theoretische Physik, Leopold-Franzens-Universität Innsbruck, A-6020 Innsbruck, Austria

⁶³NYCB Real-Time Computing Inc., Lattingtown, NY 11560-1025, USA

⁶⁴Department of Physics, Center for Cosmology and Astro-Particle Physics, The Ohio State University, Columbus, OH 43210, USA

⁶⁵Department of Chemistry and Physics, Purdue University Calumet, Hammond, IN 46323-2094, USA

⁶⁶Institut für Theoretische Physik and Astrophysik, Universität Würzburg, D-97074 Würzburg, Germany

⁶⁷Institució Catalana de Recerca i Estudis Avançats (ICREA), Barcelona, Spain

⁶⁸Consorzio Interuniversitario per la Fisica Spaziale (CIFS), I-10133 Torino, Italy

⁶⁹INTEGRAL Science Data Centre, CH-1290 Versoix, Switzerland

⁷⁰NASA Postdoctoral Program Fellow, USA

⁷¹Dipartimento di Fisica, Università di Roma “Tor Vergata”, I-00133 Roma, Italy

⁷²Praxis Inc., Alexandria, VA 22303, resident at Naval Research Laboratory, Washington, DC 20375, USA

associations, we find that the new association matches the predicted source class in $\sim 80\%$ of the sources.

Subject headings: catalogs – gamma rays: general – methods: statistical – galaxies: active – pulsars: general

1. Introduction

Astrophysical sources of high-energy γ rays (photon energies above 10 MeV), although inherently interesting as tracers of energetic processes in the Universe, have long been hard to identify. Only four of the 25 sources in the second COS-B catalog had identifications (Swanenburg et al. 1981), and over half the sources in the third EGRET catalog had no associations with known objects (Hartman et al. 1999). A principal reason for the difficulty of finding counterparts to high-energy γ -ray sources has been the large positional errors in their measured locations, a result of the limited photon statistics and angular resolution of the γ -ray observations and the bright diffuse γ -ray emission from the Milky Way. In addition, a number of the COS-B and EGRET sources were determined to be spurious by follow-up analysis and observations.

A major step forward for detection and identification of high-energy γ -ray sources came when the *Gamma-ray Large Area Space Telescope* (GLAST) was launched on 2008 June 11. It began its scientific operations two months later, and shortly thereafter, it was renamed the *Fermi* Gamma-ray Space Telescope. Its primary instrument is the Large Area Telescope (LAT; Atwood et al. 2009), the successor to the Energetic Gamma-Ray Experiment Telescope (EGRET) on the *Compton Gamma-Ray Observatory* (Thompson et al. 1993). The LAT offers a major increase in sensitivity over EGRET, allowing it to study the 100 MeV to ~ 300 GeV γ -ray sky in unprecedented detail.

The high sensitivity, improved angular resolution and nearly uniform sky coverage of the LAT make it a powerful tool for detecting and characterizing large numbers of γ -ray sources. The *Fermi*-LAT First Source Catalog (1FGL; Abdo et al. 2010a) lists 1451 sources detected during the first 11 months of operation by the LAT, of which 821 were shown to be associated with at least one plausible counterpart. Of these, 698 were extragalactic (mostly Active Galactic Nuclei, or AGNs) and 123 were Galactic (mostly pulsars and supernova remnants, but also pulsar wind nebulae and high-mass X-ray binaries). After the publication of the 1FGL catalog, the association panorama evolved very quickly with the release of the catalog of AGNs (1LAC; Abdo et al. 2010k) as well as a catalog of pulsar wind nebulae (PWNe) and supernova remnants (SNRs) (Ackermann et al. 2011).

Here, as a starting point for our multivariate classification strategy, we consider the entire original list of 630 1FGL sources that remain unassociated with plausible counterparts at other wavelengths. A plausible counterpart is a member of a known or likely γ -ray emitting class located close to the 95% uncertainty radius of a given 1FGL source, with an association confidence of 80% or

68 higher (Abdo et al. 2010a). The 95% uncertainty radii for 1FGL source locations are typically 10'.
69 While greatly improved over the degree-scale uncertainties of previous instruments, these position
70 measurements are still inadequate to make firm identifications based solely on location.

71 We have taken a multi-pronged approach toward understanding these unassociated 1FGL
72 sources, using all the available information about the γ -ray sources. Information about locations,
73 spectra, and variability has been combined with properties of the established γ -ray source classes
74 and multiwavelength counterpart searches.

75 Here we look in depth at the properties of the 1FGL unassociated sources, and investigate the
76 implications of those characteristics. Specifically, this paper addresses five primary questions:

- 77 1. What do the γ -ray properties of the unassociated 1FGL sources reveal about these sources
78 (Section 2)?
- 79 2. What does our understanding of the γ -ray properties of the associated sources suggest about
80 the possible source class for each of the 1FGL unassociated sources (Section 3)?
- 81 3. What new associations or multiwavelength counterparts have been found beyond those from
82 the first LAT catalog (Section 4)?
- 83 4. Do the new classifications properly predict sources that have been associated since the release
84 of the 1FGL catalog (Section 5)?
- 85 5. What do the new classifications and associations imply about the existence of unknown new
86 γ -ray source classes (Section 6)?

87 Although the 2FGL catalog (Abdo et al. 2011b) was being developed in parallel with the present
88 work, we focus on the 1FGL results, where some follow-up results are available for comparison with
89 the methods of this work. Such follow-up observations for 2FGL have yet to be done.

90 **2. Gamma-ray properties of unassociated *Fermi*-LAT sources**

91 In the 1FGL catalog (Abdo et al. 2010a, hereafter “1FGL”), source identifications and associa-
92 tions were assigned through an objective procedure. For a source to be considered identified in the
93 1FGL catalog, detection of periodic emission (pulsars or X-ray binaries) or variability correlated
94 with observations at other wavelengths (blazars) was required. Additionally, measurement of an
95 angular extent consistent with observations at other wavelengths was used to declare identifica-
96 tions for a few sources associated with SNRs and radio galaxies (Abdo et al. 2009d, 2010d,f,h).
97 Associations were reported only for sources with positional correlations between LAT sources and
98 members of plausible source classes (based on Bayesian probabilities of finding a source of a given
99 type in a LAT error box). This automated procedure was based on a list of 32 catalogs that contain

100 potential counterparts of LAT sources based either on prior knowledge about classes of high-energy
 101 γ -ray emitters or on theoretical expectations. In addition, it indicated coincident detections at
 102 radio frequencies and TeV energies, as well as positional coincidences with EGRET and *AGILE*
 103 sources.

104 In total 821 of the 1451 sources in the 1FGL catalog (56%) were associated with a least one
 105 counterpart by the automated procedure, with 779 being associated using the Bayesian method
 106 while 42 are spatially correlated with extended sources based on overlap of the error regions and
 107 source extents. From the simulations in 1FGL we expect that ~ 57 among the 821 sources (7%) are
 108 associated spuriously in 1FGL. We found the initial list of unassociated sources by simply extracting
 109 the list of 1FGL sources without any association from the 1FGL catalog. These sources are spread
 110 across the sky, with about 40% located within 10° of the Galactic plane.

111 Sources without firm identifications that are in regions of enhanced diffuse γ -ray emission along
 112 the Galactic plane or are near local interstellar cloud complexes (like Orion), sources that lie along
 113 the Galactic ridge ($300^\circ < l < 60^\circ$, $|b| < 1^\circ$), and sources that are in regions with source densities
 114 great enough that their position error estimates overlap in the γ -ray data are called c-sources,
 115 as their 1FGL designator has a “c” appended to indicate “caution” or “confused region”. The
 116 remainder of the unassociated sources did not have a “caution” designator in 1FGL, and here are
 117 called “non-c” sources.

118 The positions, variability and spectral information given in the catalog provide an important
 119 starting point for the characterization of LAT unassociated sources. We can easily compare intrinsic
 120 properties of the 1FGL sources such as spectral index, curvature index and flux in different energy
 121 bands for both associated and unassociated populations, potentially providing insight into the likely
 122 classes of the unassociated sources.

123 For the 1FGL catalog, the limiting flux for detecting a source with photon spectral index
 124 $\Gamma = 2.2$ and Test Statistic of 25 ($TS = 2\Delta\log(\text{likelihood})$ Mattox et al. 1996) varied across the sky
 125 by about a factor of five (see Figure 19 of 1FGL). This non-uniform flux limit is due to the non-
 126 uniform Galactic diffuse background and non-uniform exposure (mostly arising from the passage
 127 of the *Fermi* observatory through the South Atlantic Anomaly).

128 As discussed in 1FGL, when the variability and spectral curvature properties of *Fermi*-LAT
 129 sources are compared against each other, a clear separation is visible between bright sources with
 130 AGN associations and those with pulsar associations. In Figure 1 (top panel), pulsars lie in the
 131 lower right-hand quadrant and AGN lie in the upper half. However, in the lower left-hand quadrant
 132 the two classes mix, making it difficult to distinguish between them. This region of parameter space
 133 is home to much of the unassociated source population (bottom panel). A closer look at these and
 134 other properties of the known sources gives clues to methods of separating the two major types,
 135 allowing us to classify some of the unassociated sources as likely members of one of these two source
 136 types (Section 3).

2.1. Source locations and Flux distributions

137

138 The spatial distributions of the major source types (AGN, pulsars, unassociated sources) are
 139 given in Table 1. It is clear that there is a significant excess of unassociated sources at low Galactic
 140 latitudes ($|b| < 10^\circ$) where 63% of the detected sources have no formal counterparts, compared to
 141 only 36% unassociated at $|b| > 10^\circ$.

142

Figure 2 shows the spatial distribution of LAT unassociated sources, with the positions of non-
 143 c sources shown as crosses and the c-source positions given by circles. As for the EGRET (3EG)
 144 catalog sources, the distribution is clearly not isotropic (Hartman et al. 1999). One consideration
 145 when interpreting the distribution of unassociated 1FGL sources is that a number of the remaining
 146 unassociated sources are in low Galactic latitude regions where catalogs of AGNs have limited or
 147 no coverage, reducing the fraction of AGN associations. If we bin the different source types by
 148 Galactic latitude (Figure 3), we see a clear absence of AGN associations in the central 10° of the
 149 Galaxy ($|b| < 5^\circ$), while in the same region there is a spike in the number of unassociated sources.

150

The unassociated sources have an average flux of 3.1×10^{-9} ph cm $^{-2}$ s $^{-1}$ ($E > 1$ GeV), while
 151 the associated population averages are 5.5×10^{-8} ph cm $^{-2}$ s $^{-1}$ for pulsars and 2.7×10^{-9} ph cm $^{-2}$
 152 s $^{-1}$ for AGN.

153

In the Galactic plane a γ -ray source must be brighter than at high latitudes in order to be
 154 detected above the strong Galactic diffuse emission. Figure 4 (left panel) shows the 1FGL source
 155 flux distribution versus Galactic latitude for three longitude bands. It is clear that the Galactic
 156 plane ($|b| < 2.5^\circ$) is dominated by Galactic diffuse emission, raising the flux detection threshold
 157 to $> 5 \times 10^{-9}$ ph cm $^{-2}$ s $^{-1}$. This is reflected in the average flux of the unassociated c-sources
 158 which at 8.2×10^{-9} ph cm $^{-2}$ s $^{-1}$ is significantly higher than that for the non-c unassociated source
 159 population (1.7×10^{-9} ph cm $^{-2}$ s $^{-1}$). Outside the central region of the Galaxy, the flux threshold
 160 is lower than that shown in Figure 4.

161

As was the case for COS-B and EGRET, it is likely that a subset of the unassociated sources
 162 are spurious, resulting from an imperfect Galactic diffuse model. Such sources probably have very
 163 low significance, poor localization, and a spectral shape that mimics that of the Galactic diffuse
 164 emission itself. The c-sources in the 1FGL catalog are candidates to be sources of this type.

165

As discussed in Section 4.7 of 1FGL, the latitude distribution of the Galactic ridge ($300^\circ <$
 166 $l < 60^\circ$) unassociated sources shows a sharp narrow peak in the central degree ($|b| < 0.5^\circ$) of the
 167 Galaxy (Figure 4, right). If this feature is not an artifact, and we assume these sources originate
 168 in a Galactic population, then the scale height for this population must be ~ 50 pc, to keep the
 169 average distance to the sources within the Galaxy. Such a scale height does not correspond to any
 170 known population of γ -ray sources, making it likely that a number of the sources in the Galactic
 171 ridge are spurious.

2.2. Spectral properties

172

173 The 1FGL catalog provides spectral information that may be useful for distinguishing between
 174 different source classes. As part of the 1FGL analysis all sources were fit with a power-law spectral
 175 form and the spectral indices were included in the catalog. In addition, the catalog includes a
 176 “curvature index”, which measures the deviation of the spectrum from the simple power-law form
 177 for each source. This means the curvature index is more a measure of the quality of the power-law
 178 spectral fit than of the intrinsic spectral shape. Figure 5 shows the distributions of the spectral index
 179 (top panel) and curvature index (middle panel) with respect to flux. Neither of these parameters
 180 appears to discriminate well between the AGN and pulsar populations. In addition, the relationship
 181 is nearly linear for the curvature index, indicating that this parameter is strongly correlated with
 182 flux. That is, fainter sources have relatively poorly measured spectra that cannot be measured
 183 to be significantly different from power laws. This means that faint γ -ray sources provide less
 184 discriminating information than bright sources.

185 The majority of γ -ray AGN are blazars, which are relativistic jet sources with the jets directed
 186 toward the earth. An important property of blazars is their typical γ -ray spectral index, which
 187 offers some discrimination power between FSRQs (Flat Spectrum Radio Quasar) and BL Lacs
 188 (Abdo et al. 2010j). The spectra of blazars in both of these sub-classes are typically well described
 189 as broken power laws in the LAT energy range, and the distributions of spectral indices for FSRQs
 190 and BL Lacs are compatible with Gaussians (Abdo et al. 2009a, 2010k). However, because pulsar
 191 spectra are not well described by power-laws, the spectral index of a power-law fit is not a good
 192 discriminator between pulsar and AGN classes.

193 As mentioned before, Figure 5 (middle) shows that the curvature index for pulsars is strongly
 194 correlated with flux. This is primarily because many of the pulsars detected in the 1FGL catalog are
 195 strong γ -ray sources, with brighter pulsars having a more significant spectral curvature than fainter
 196 pulsars. Unfortunately, the broken power-law spectral forms of bright blazars (e.g., Ackermann
 197 et al. 2010) also have the effect of inducing a correlation between curvature index and flux for LAT
 198 blazars.

199 There are few sources with significant detections in all of the five spectral bands used to
 200 calculate the curvature index. Only 36 of the 630 unassociated sources are strongly-enough detected
 201 to have flux measurements reported in each band in the 1FGL catalog, as this requires a $TS > 10$
 202 in each energy range. By contrast, 181 of the unassociated sources are detected in only a single
 203 band, with an additional 88 sources having upper limits in all the spectral bands (i.e., are only
 204 detected when data at all energies are combined).

2.3. Variability properties

In the 1FGL catalog the variability index for each source was defined as the χ^2 of the deviations of eleven monthly (30-day) source flux measurements from the average source flux (Abdo et al. 2010a). While this value increases with flux for AGN, it does not do so for the pulsars (Figure 5, bottom panel), making variability a much better discriminator between the two major classes. One property of blazars is that they are frequently significantly variable in γ rays (Abdo et al. 2010g). Their fluxes can vary up to a factor of five on time scales of a few hours and by a factor of 50 or more over several months. As a consequence, their characteristic variability can serve as a primary discriminator. This property has been used to turn some *Fermi*-LAT AGN associations into identifications due to their timing properties (Abdo et al. 2010g; Vandenbroucke et al. 2010). For variability to be a useful indicator, the time scale must be adapted to the source significance. Indeed, for a faint source, the variability needs to be tested on longer time scales than for a bright source. All sources in the 1FGL catalog were processed in the same way, regardless of flux. Thus, for the many 1FGL sources not bright enough to be significantly detected on monthly time scales the 1FGL variability index is not a sensitive discriminator of variability.

Pulsars, on the other hand, are generally steady sources. Where variability has been seen in γ rays, it has been attributed to flares in the nebular contribution of a PWN, rather than to the pulsar itself (Tavani et al. 2011; Abdo et al. 2011c). This flux stability places pulsars in extreme opposition to AGN in the γ -ray regime. Essentially any significant detection of variability in an unassociated source is enough to make a pulsar classification extremely unlikely.

In the 1FGL catalog, 241 sources were found to be variable at a formal confidence level of 99% (variability index > 23.21). Of these, 2 are HMXBs, 221 are AGN, and 18 are unassociated. Variability in bright sources is easier to detect as the source flux is typically above the sensitivity threshold in each monthly bin. For the lower-flux unassociated sources, however, we need a method to improve the detection of variability. Using the fractional variability (discussed in Section 3.1, is one such method.

2.4. Comparison with source modeling

We can also examine what source distributions we might expect given the populations of source types in 1FGL. We do this by first estimating the total number of detected AGN in 1FGL, which we derive from a model population. To quantify the total number of AGN, we model the population and then apply that model to the 1FGL catalog.

We use the *Fermi*-LAT Log N -Log S distribution (the distribution of the number N of sources detectable at a given sensitivity S) for AGN (Abdo et al. 2010j), and the 1FGL sensitivity map (Figure 19 of Abdo et al. 2010a) to generate a Galactic map that contains the number of the expected AGN at each position in the sky. Summing these results over Galactic longitude we

240 obtain the AGN latitude profile shown in Figure 6. Integrating the AGN model allows us to
 241 estimate the number of expected AGN in the sky. By subtracting the number of AGN found by
 242 the model from the sources in the 1FGL catalog we obtain the number of Galactic sources in and
 243 out of the plane. This gives the Galactic source estimates for the unassociated source list.

244 Table 2 compares the 1FGL source counts with this model for low and high-latitude regions.
 245 It is clear that the group of sources that is most difficult to associate are those of Galactic origin
 246 at low Galactic latitudes. This is likely due to the presence of a population of spurious sources in
 247 that region in the 1FGL catalog.

248 At high Galactic latitudes, pulsars are the second most numerous class of identified γ -ray
 249 sources; most of those are millisecond pulsars (MSPs). From the set of 1FGL pulsars and the new
 250 pulsar associations discussed herein, we find that more than a third of the γ -ray pulsars known to
 251 date are MSPs. If we then assume that $\sim 50\%$ of the 271 unassociated sources that are expected
 252 to be Galactic sources are pulsars (based on the fraction of Galactic sources which are pulsars as
 253 given in Table 1), and one third of those pulsars are MSPs, we find that we expect 45 new MSPs
 254 in the 1FGL unassociated source list. Of the 31 new MSPs discovered to date (Section 4.2), 28 are
 255 at high Galactic latitudes, suggesting that an expected number of 45 is not unreasonable.

256 At low Galactic latitudes the source content is more diverse, with half the sources being
 257 compact objects (pulsars and X-ray binaries) and nearly half being extended sources (SNRs and
 258 PWNe). If the unassociated sources have a similar distribution, then there will be ~ 100 pulsars
 259 and ~ 100 SNRs/PWNe.

260 3. Classification of unassociated sources

261 The spatial, spectral and variability properties discussed in Section 2 provide a framework that
 262 allows us to try to predict the expected source classes for the sources that remain unassociated.
 263 This is done by using the properties of the associated sources to define a model that describes the
 264 distributions and correlations between measured properties of the γ -ray behavior of each source
 265 class. This model is then compared to the γ -ray properties of each unassociated source. Generating
 266 the model requires an associated source parent population with enough members to describe the
 267 behavior well. For this reason, we have focused only on AGN and pulsars as the input source
 268 populations.

269 To create a model, it is necessary to use γ -ray properties that are clearly different between the
 270 parent populations. For 1FGL, the best parameters are the spectral index, curvature index, and
 271 variability index, as well as hardness ratios between the different spectral bands. In addition, it is
 272 important that the properties used to generate the model not be related to source significance, as
 273 this will bias the results. However, as discussed in Section 2.1, the curvature index appears to be
 274 dependent on the source flux, and thus is not a good indicator of the parent population. Also, the
 275 spectral index and hardness ratios are both spectral indicators, so they overlap in functionality.

276 Since the hardness ratios provide more information about spectral shape than the spectral index,
 277 they are preferred for this analysis.

278 To generate valid classifications, we must first define new parameters that allow intrinsic prop-
 279 erties to be compared rather than relative fluxes. With the new parameters in hand, we can
 280 generate classification predictions using multiple methods, and compare these predictions to each
 281 other. However, the results from these techniques assume that the training samples and test sam-
 282 ples have the same distributions of intrinsic properties. This is not true for the 1FGL unassociated
 283 sources, as they are more frequently found in the plane of the Galaxy with elevated background
 284 levels and in confused regions. To help compensate for this difference, we will validate the results
 285 against an independent set of classified sources.

286 3.1. Improving source type discriminators

287 To mitigate the effect of low fluxes on the determination of the band spectra, it is necessary
 288 to define additional comparative parameters that remove the significance dependency. In this case,
 289 the 1FGL catalog provides a set of fluxes in five bands for each source from which we can find
 290 hardness ratios. To get a normalized quantity the hardness ratios are constructed as:

$$HR_{ij} = (EnergyFlux_j - EnergyFlux_i) / (EnergyFlux_j + EnergyFlux_i) \quad (1)$$

291 This quantity will always be between -1 and 1 ; -1 for a very soft source ($[high]EnergyFlux_j =$
 292 0) and $+1$ for a very hard source ($[low]EnergyFlux_i = 0$). Here energy flux in $\log(E)$ units (i.e.
 293 νF_ν) is used instead of photon flux because the definition works well only when the quantities are
 294 of the same order. This is true for the energy fluxes (because the spectra are not too far from a
 295 E^{-2} power law) but not for photon fluxes.

296 It is also possible to define a quantity that discriminates curvature by combining two hardness
 297 ratios, preferably from bands with a high number of detected sources. Here we use $(HR_{23} - HR_{34})$,
 298 where bands 2, 3, and 4 are for 0.3–1, 1–3, and 3–10 GeV respectively. This hardness ratio
 299 difference, or curvature, is positive for spectra curved downwards in νF_ν (like pulsars), zero for
 300 power laws and negative for spectra curved upwards (with a strong high-energy component).

301 To remove the source significance dependency for variability, we use the fractional variability
 302 (as defined in Equation 5 of Abdo et al. 2010a) instead of the variability index. The fractional
 303 variability is:

$$FracVar = \sqrt{\frac{\sum_i (Flux_i - Flux_{av})^2}{(N_{int} - 1) Flux_{av}^2} - \frac{\sum_i \sigma_i^2}{N_{int} Flux_{av}^2} - f_{rel}} \quad (2)$$

304 where N_{int} is the number of time intervals (11 in 1FGL), σ_i is the statistical uncertainty in F_i , and
 305 f_{rel} is an estimate of the systematic uncertainty on the flux for each interval. (Here we use 3% as in
 306 1FGL.) For some 1FGL sources the quantity inside the square root is negative. Those sources are

307 assigned a fractional variability of 2%. Figure 7 shows fractional variability versus the curvature
308 ($HR_{23} - HR_{34}$) for both the associated (top panel) and unassociated (bottom panel) 1FGL sources.

309 To allow the largest possible sample when performing the classification, we use the actual best
310 fit values in calculating both these quantities, even when the 1FGL analysis reported only 2-sigma
311 upper limits. For such sources the variable is not well constrained. However, it will contribute to
312 the distribution used to determine the classifications and may provide a small amount of additional
313 discriminating power.

314 **3.2. Classification using Classification Trees**

315 We have implemented two different data mining techniques to determine likely source classifica-
316 tions for the 1FGL unassociated sources: Classification Trees (this section) and Logistic Regression
317 (Section 3.3). Both techniques use identified objects to build up a classification analysis which
318 provides the probability for an unidentified source to belong to a given class. We applied these
319 techniques to the sources in 1FGL to provide a set of classification probabilities for each unidentified
320 source.

321 Classification Trees are a well-established class of algorithms in the general framework of data
322 mining and machine learning (Breiman et al. 1984). The general principle of machine learning
323 is to train an algorithm to predict membership of cases or objects to the classes of a dependent
324 variable from their measurements on one or more input variables. The advantage of this class of
325 algorithms is the ability to produce a unique predictor parameter that takes into account several
326 input quantities simultaneously. Other well-known flavors of machine learning algorithms include
327 artificial neural networks, support vector machines and bayesian networks.

328 The purpose of analyses via tree-building algorithms is to determine a set of *if-then* logical
329 conditions (called tree-nodes) that permit accurate prediction or classification of cases: the training
330 procedure generates a tree in which each decision node contains a test on some input variable's
331 value. The trees in this analysis are built through a process known as binary recursive partitioning,
332 which is an iterative process of splitting the data into partitions. Initially all the records in the
333 training set are assigned to a single class: the algorithm then tries breaking up the data, using
334 every possible binary split on every field. The peculiar advantage of Classification Trees for our
335 specific application is their flexibility in handling sparse or uneven distributions.

336 The specific flavor of algorithm used in this case was Adaptive Boosting, which reweights the
337 importance of input sources at each step of the classification. The training of boosted decision trees
338 is a recursive procedure, whereupon the weights of each incorrectly classified example are increased
339 at each step, so that the new classifier focuses more on those examples. The output of such a
340 procedure is actually a collection of trees, all grown from the same input sample: the selection will
341 be done on a majority vote on the result of several decision trees (200 in the present case). In the
342 following text, we will always refer to a single Classification Tree for simplicity, even though the

343 real classifier is a much more complex object.

344 The training and application of Classification Trees to this specific analysis has been performed
 345 using TMine, an interactive software tool for processing complex classification analyses developed
 346 within the Fermi-LAT collaboration (Drlica-Wagner & Charles 2011). TMine is based on ROOT
 347 (Brun & Rademakers 1997), a very popular data analysis framework for high energy physics exper-
 348 iments. For the processing and parallel evaluation of multivariate classification algorithms, TMine
 349 utilizes the ROOT Toolkit for Multivariate Analysis (TMVA) (Hocker et al. 2007).

350 3.2.1. Selection of the relevant training variables

351 The first step of the CT analysis is to select a sample of data to build the predictor variable.
 352 We decided to focus on the two most abundant classes of objects in the *Fermi* catalog, AGN and
 353 pulsars, and to train a Classification Tree to discriminate between them. We trained a predictor
 354 using all the associated AGNs and pulsars in the 1FGL catalog (Abdo et al. 2010a). Because
 355 of the spectral similarities with pulsars, potential associations for sources near SNRs have been
 356 compounded with the pulsars sample. The output of this training process is a parameter (the
 357 predictor) which describes the probability for a new source to be an AGN.

358 Choosing the most appropriate set of variables for training the Classification Tree is a very
 359 delicate step in the analysis. It is extremely important to ensure that the selected variables are not
 360 dependent on the flux, the location or the significance of the source: this check can be accomplished
 361 by comparing the distribution of the various parameters for associated and unassociated sources.
 362 Physical considerations about the γ -ray properties of each source class also guided us in the choice
 363 of the most effective variables for discriminating AGN from pulsars (Section 3.1).

364 After exploring most of the parameters in the 1FGL catalog, we selected a set of variables
 365 that includes: the curvature (HR_{23} - HR_{34}), the spectral index and the fractional variability of
 366 each source, plus the Hardness Ratios for the 5 energy bands in the catalog. Table 3 ranks the
 367 relative importance of the different variables at distinguishing AGNs from pulsars: the weight of
 368 each variable was computed by the Classification Tree algorithm during the training process.

369 As described in section 3.1, we used for training the actual best fit values for each variable,
 370 even when the 1FGL analysis reported only upper limits. In case of faint sources that are not
 371 detected in one of the energy bands, some of the Hardness Ratios will be very close to -1 or 1: this
 372 is when the ability of Classification Trees in handling sparse distributions is particularly useful.
 373 Similar considerations apply to the fractional variability, which is very close to zero for pulsars, but
 374 varies for AGNs.

375 We chose not to use the Galactic latitude as input to the CT in order to avoid biasing our
 376 selection against AGN situated along the Galactic plane and pulsars (especially MSPs) situated
 377 at high Galactic latitude. Furthermore, this choice gives us the opportunity to use the latitude

378 distributions of the different populations as a cross check of our result. (The new pulsar candi-
 379 dates should be mainly distributed along the Galactic plane, while the AGN candidates should be
 380 isotropically distributed).

381 While training the Classification Tree, 30% of known AGNs and pulsars, randomly selected
 382 from the input sample, were kept aside for cross-validation of the method. Such cross-validation
 383 was performed by comparing the predictor distributions for the training and testing samples via a
 384 Kolmogorov-Smirnov test. The result of the test provides a 93% probability for the AGN distribu-
 385 tions and a 47% probability for the pulsar distributions, which make the test fully satisfactory.

386 It must also be noted that the sources associated with a different class than AGN or pulsar
 387 have been excluded from this training procedure, for a total of 24 sources. We cannot treat these
 388 24 sources uniformly as “background”, because of the smallness of their sample and the diversity
 389 of their spectral properties. However, it is possible to estimate the contamination to the candi-
 390 date AGN and pulsar samples deriving from the likely presence of these “other” sources in the
 391 unassociated sample.

392 3.2.2. Output of the Classification Procedure

393 The second step of the analysis consists of deriving the predictor variable for unassociated
 394 sources by applying the Classification Tree that was trained in the previous step. The resulting
 395 predictor is a parameter that describes the probability that each of the unassociated sources is
 396 an AGN. The predictor is included in Table 4 which lists all 630 unassociated *Fermi*-LAT 1FGL
 397 sources, and combines results for all the analyses discussed within this paper.

398 Figure 8 shows the distribution of the predictor for the 1FGL associated sources used in the
 399 training of the tree (left panel) and the distribution of the predictor for the unassociated sources
 400 (right panel). The global shapes of the two distributions are clearly different, with an apparent
 401 excess of pulsar-like sources among the unassociated sources when compared to the associated
 402 source distribution. This may be due to the presumably different fractions of AGN and pulsars in
 403 the associated and unassociated samples, or there may be an additional contributing component.
 404 Nevertheless, the distribution of associated sources clearly shows that we can select a set of AGN
 405 and pulsar candidates with high confidence, when choosing the appropriate fiducial regions.

406 We set two fiducial thresholds: all the sources with a predictor greater than 0.75 are classified
 407 as AGN candidates while all the sources with a predictor smaller than 0.6 are classified as pulsar
 408 candidates. All the sources with an intermediate value of the predictor remain unclassified after
 409 the CT analysis. The choice of these boundaries is optimized for an efficiency of 80% for the two
 410 source classes in order to keep the misclassification fraction under 2% (the misclassified fraction for
 411 a certain efficiency is determined by the width of the predictor distribution). Here, 80% of AGN
 412 associations in 1FGL have a predictor greater than 0.75 and 80% of pulsars have a predictor smaller
 413 than 0.6.

414 In this case, the extrapolation from the value of the predictor to the probability of class
 415 membership was performed empirically from the combined input sample (which includes both
 416 the training and testing samples). The expected misclassification fraction in each class was also
 417 evaluated with the same method. This analysis was repeated using the training and testing samples
 418 separately and yielded identical results. A more complex study used the area under the Receiver-
 419 Operating-Characteristic (ROC) curve that is obtained by plotting all combinations of true positives
 420 and the proportion of false negatives generated by varying the decision threshold. This study
 421 provided similar extrapolation results, but more optimistic misclassification fractions: we therefore
 422 decided to rely on the more conservative misclassification estimation provided by the combined
 423 input sample.

424 The predictor distribution for the 24 sources that were not used during the training procedure
 425 can be used to estimate the further contamination from these sources to the AGN and pulsar
 426 candidate distributions: we expect that up to 2% of the newly classified AGN candidates and up
 427 to 4% of the newly classified pulsar candidates will indeed belong to one of the "other" classes
 428 (galaxies, globular clusters, supernova remnants, etc.).

429 3.3. Classification using Logistic Regression

430 Another approach to assign likely classifications for the 1FGL unassociated sources is the
 431 Logistic Regression (LR) analysis method (Hosmer & Lemeshow 2000). Unlike the CT analysis,
 432 LR allows us to quantify the probability of correct classification based on fitting a model form to
 433 the data.

434 LR is part of a class of generalized linear models and is one of the simplest data mining
 435 techniques. LR forms a multivariate relation between a dependent variable that can only take
 436 values from 0 to 1 and several independent variables. When the dependent variable has only
 437 two possible assignment categories, the simplicity of the LR method can be a benefit over other
 438 discriminant analyses.

439 In our case, the dependent variable is a binary variable that represents the classification of
 440 given 1FGL unassociated source. Quantitatively, the relationship between the classification and its
 441 dependence on several variables can be expressed as:

$$P = \frac{1}{(1 + e^{-z})} \quad (3)$$

442 where P is the probability of the classification, and z can be defined as a linear combination:

$$z = b_0 + b_1x_1 + b_2x_2 + \dots + b_nx_n \quad (4)$$

443 where b_0 is the intercept of the model, the b_i ($i = 0, 1, 2, \dots, n$) are the slope coefficients of the
 444 LR model and the x_i ($i = 0, 1, 2, \dots, n$) are the independent variables. Therefore, LR evaluates

445 the probability of association with a particular class of sources as a function of the independent
 446 variables (e.g. spectral shape or variability).

447 Much like linear regression, LR finds a “best fitting” equation. However, the principles on
 448 which it is based are rather different. Instead of using a least-squared deviations criterion for
 449 the best fit, it uses a maximum-likelihood method, which maximizes the probability of matching
 450 the associations in the training sample by optimizing the regression coefficients. As a result, the
 451 goodness of fit and overall significance statistics used in LR are different from those used in linear
 452 regression.

453 *3.3.1. Selection of the training sample and the predictor variables*

454 As LR is a supervised data mining technique, it must be trained on known objects in order to
 455 predict the membership of a new object to a given class on the basis of its observables. As with CT
 456 analysis, we trained the predictor using the pulsar and AGN associated sources in the 1FGL catalog
 457 (Abdo et al. 2010a). Like the CT analysis, the output of this training process is the probability
 458 that an unidentified source has characteristics more similar to an AGN than to a pulsar.

459 To evaluate the best predictor variables for the LR analysis, we used the likelihood ratio test,
 460 comparing the likelihoods of the models not including (null hypothesis) and including (alternative
 461 hypothesis) the predictor variable under examination. We started by using the fractional variability,
 462 the spectral index, the hardness ratios for the 5 energy bands in the catalog and the position on the
 463 sky (i.e. the Galactic latitude and longitude). The value of the likelihood ratio test is the p-value,
 464 and is useful in determining if a predictor variable is significant in distinguishing an AGN from
 465 a pulsar. If the p-value for a given predictor variable is smaller than the significance threshold α
 466 (0.05) then the predictor variable is included in the multivariate LR model. We did not include
 467 the curvature value ($HR_{23} - HR_{34}$) in this evaluation because the LR analysis does not work well
 468 with predictor variables that are linearly dependent on other predictor values.

469 We then calculated the significance of each predictor variable to find the resulting LR coeffi-
 470 cients. The list of the LR predictor variables with the relative values of the maximum likelihood
 471 ratios can be found in Table 5.

472 While AGN are isotropically distributed and pulsars are concentrated along the Galactic plane,
 473 we wanted to see whether our multivariate LR model was able to recognize this effect. The results
 474 indicate that Galactic latitude and longitude are not significant at the $\alpha = 0.05$ (5% significance)
 475 level. Moreover we find that also HR_{12} is not highly significant in the LR analysis. It is interesting
 476 to note that HR_{12} , in the univariate LR model, is quite significant (p-value=0.02) to distinguish
 477 between AGNs and pulsars but in a multivariate LR analysis it loses its significance. In Table 5
 478 those predictor variables selected for the LR model are above the line and those we did not select
 479 lie below the line.

3.3.2. *Defining thresholds*

480

481 Next we derive the predictor variable for 1FGL unassociated sources by applying the trained
 482 classification analysis to those sources. Since the LR analysis used AGNs as primary source type,
 483 the output parameter (A) listed in Table 4 describes the probability that an unassociated source
 484 is an AGN. The probability that an unassociated source is a pulsar is $P = 1 - A$ (because we are
 485 modeling the behavior of AGNs as “opposite” of the behavior of the pulsars based on the predictor
 486 variables).

487 In principle, the dependent variable is a binary variable that represents the presence or absence
 488 of a particular class of objects. We could have selected “pulsars” and “non-pulsars” (e.g. all other
 489 1FGL associated sources) to teach the model to recognize the new pulsars, and done similarly for
 490 the AGNs. We did not follow this approach because there are no source populations in 1FGL other
 491 than AGNs and pulsars with sufficient numbers to significantly affect the results. By focusing on
 492 “opposing” characteristics, we improve the efficiency of classifying new AGN or pulsar candidates.

493 As with the CT analysis we defined two threshold values, one to classify an AGN candidate
 494 (C_A) and one to classify a pulsar candidate (C_P). We chose these two thresholds by analyzing the
 495 ROC curves so that 80% of the AGN associations in 1FGL would have a predictor value greater
 496 than C_A and 80% of the pulsars would have a predictor value smaller than C_P , and to result in very
 497 low contamination. Using this principle we set C_A to 0.98 and C_P to 0.62. With these thresholds,
 498 only 1% of AGNs are misclassified as pulsars, while 3% of pulsars are classified as AGN.

499 To estimate how accurately our predictive model performs in practice, we cross-validated using
 500 only the 756 pulsars and AGNs in the 1FGL catalog. We held out 75 sources to be the testing
 501 data set, and we used the remaining 681 for training. We repeated this procedure 10 times, using
 502 a different set of 75 test sources in each data set. At the end, this 10-fold cross-validation showed
 503 that the average testing efficiency rates for these threshold values are 75% for pulsars and 80% for
 504 AGNs, and that the average testing error rates (false positives) are very low, 0.05% for pulsars and
 505 0.02% for AGNs. The 5% lower success rate for the pulsars is likely due to low statistics in the test
 506 samples.

507 If we apply the model to the 1FGL unassociated sources we find that 368 are classified as
 508 AGN candidates ($P > 0.98$), 122 are classified as pulsar candidates ($P < 0.62$) and 140 remain
 509 unclassified after the LR analysis. The distributions of 1FGL associated and unassociated sources
 510 as a function of the probability of being pulsars are shown in the Figure 9. The thresholds for
 511 assigning pulsar candidates and AGN candidates are indicated in the figure. It is important to
 512 note that in order to meet the acceptance threshold of 80% of the known pulsars, we are including
 513 a large range of predictor values with very few pulsars. This may result in over-predicting the
 514 number of pulsars in unassociated sources.

515

3.4. Combining the two classification methods

516

517

518

519

520

521

522

523

The two classification techniques gave somewhat different results. Of the 630 unassociated sources in 1FGL, both techniques agreed on the appropriate classification for 57.6% of the sources (363), while they gave conflicting classifications for 5.4% (34 sources). The remaining 253 sources were left unclassified by one or both techniques (see Table 6). Studies comparing these classification techniques (Perlich et al. 2003) have indicated that in data sets with good separability between the discriminating characteristics, the CT analysis should provide a more robust result. However, it is evident from the right panels of Figures 8 and 9 that the signal to noise for the unassociated sources does not provide such clear separability.

524

525

526

Since the purpose of this analysis is to provide candidate sources for follow-up multiwavelength studies, we use the positive results from both techniques to generate our candidate lists. From these two methods we can synthesize a final set of classifications for each source, where:

527

528

529

530

531

532

533

- AGN candidates must be classified by at least one method, and the other method must not disagree (that is, not classify it as a pulsar).
- Pulsar candidates must be classified by at least one method, and the other method must not disagree (that is, not classify it as an AGN).
- Unclassified sources are not classified by either method.
- “Conflicting” sources are those that have been assigned opposite classifications (one AGN and one pulsar) by the two different methods

534

535

536

537

538

539

540

Based on these definitions, there are 396 AGN candidates (269 are classified as AGN by both methods), 159 pulsar candidates (72 classified as pulsars by both methods), 41 unclassified sources, and 34 conflicting sources in the 1FGL unassociated source list. Figure 10 shows the curvature-variability distribution of the newly classified AGN and pulsar candidates based on this synthesis of the two methods. We see that the unassociated sources have been separated into two populations with some overlap between them. Comparing this distribution to Figure 1 (top panel), we see that this separation follows the separation seen between the associated AGN and pulsars.

541

4. Recent association efforts

542

543

544

545

In order to validate the results of the classification methods, we must obtain an independent set of associations from those used to train the two methods. For this, we look to association efforts that have taken place since the release of the 1FGL catalog. This section will present the new associations, while the classification validation is reported in Section 5.

546 The associations listed in 1FGL were based on likely γ -ray-producing objects, i.e. those with
 547 energetic, non-thermal emission. The first LAT catalog of Active Galactic Nuclei (AGN) published
 548 shortly afterward found high-confidence AGN associations for 671 high Galactic latitude 1FGL
 549 sources, with an additional 155 LAT sources included in the low-latitude and lower confidence
 550 association lists (1LAC; Abdo et al. 2010k). The 1LAC association method was the same as for
 551 1FGL, but the acceptance threshold for association was lower than for 1FGL.

552 For the unassociated sources in this paper, which by definition do not have plausible coun-
 553 terparts among the candidate catalogs used for comparison with the LAT sources, we must look
 554 beyond the obvious candidate source classes. Even with the improved source locations provided by
 555 the *Fermi*-LAT, however, positional coincidence with a particular object is insufficient to claim an
 556 association.

557 If potential candidates can be found, then additional tests, based on spatial morphology, cor-
 558 related variability, or physical modeling of multiwavelength properties, offer the opportunity to
 559 expand the list of associations. X-ray, optical, or radio candidate counterparts all have better lo-
 560 calizations than the γ -ray sources, so that a candidate in one of these wavelength bands can be
 561 matched with those in others. Also, most (if not all) of the catalogs and observations used here to
 562 find new associations are not complete surveys of the sky. Therefore the lack of an association for
 563 a 1FGL source does not mean that the source cannot be associated. In this section we present only
 564 a preliminary report of the results from the many ongoing efforts to observe these fields in other
 565 wavebands.

566 4.1. Radio searches for AGN

567 The first step in searching for (or excluding) AGN counterparts of *Fermi*-LAT unassociated
 568 sources is to consult catalogs of radio sources. Almost all radio AGN candidates of possible interest
 569 are detected either in the NRAO VLA Sky Survey (NVSS; Condon et al. 1998) or the Sydney
 570 University Molonglo Sky Survey (SUMSS; Bock et al. 1999). NVSS covers the entire $\delta > -40^\circ$ sky
 571 and provides interferometric flux density measurements at 1.4 GHz. SUMSS covers the remainder
 572 of the sky and offers interferometric measurements at 0.843 GHz.

573 In order to discover AGN counterparts, which are radio sources with compact, flat-spectrum
 574 cores, we follow the approach of the Cosmic Lens All Sky Survey (CLASS; Myers et al. 2003; Browne
 575 et al. 2003) and the Combined Radio All-Sky Targeted Eight GHz Survey (CRATES; Healey
 576 et al. 2007)—both of which have been shown (Abdo et al. 2009a, 2010k) to include substantial
 577 numbers of radio counterparts of LAT blazars—and pursue 8.4 GHz follow-up interferometry of
 578 blazar candidates. The *Fermi*-motivated VLA programs AH976 (Healey et al. 2009) and AH996 (in
 579 progress) obtained such data for several hundred sources, and ~ 50 of these appear as “affiliations”
 580 (i.e., candidate counterparts for which quantitative association probabilities could not be computed)
 581 in the 1LAC catalog. 108 new associations, including the “figure of merit” value for each association

582 (Abdo et al. 2010k), were determined by these VLA follow-up programs.

583 Recently, serendipitous radio identification surveys of 1FGL sources have been independently
 584 carried out using the recently released Australia Telescope 20 GHz radio source catalog (Murphy
 585 et al. 2010) which contains entries for 5890 sources observed at $\delta < 0^\circ$. Cross-correlation between
 586 the 1FGL source list and the AT20G catalog has been performed by Mahony et al. (2010) and
 587 Ghirlanda et al. (2010). In particular, Mahony et al. (2010) find correlated radio sources for 233
 588 1FGL sources and, based on Monte Carlo tests, they infer that 95% of these matches are genuine
 589 associations. While most of these radio detections are not identified or classified as specific object
 590 types, nine of the sources are considered likely to be AGNs (based on their properties at radio
 591 frequencies). Ghirlanda et al. (2010) obtain a similar number of matches with the AT20GHz
 592 catalog (~ 230) and propose eight of the same sources as likely AGN. All but one of these new
 593 associations were also found by the VLA observing program.

594 To date, radio observations of sources in the 1FGL unassociated sample have produced 109
 595 new AGN associations. These new AGN associations are included in Table 7. In addition, the
 596 1LAC catalog documented 57 other AGN associations with 1FGL unassociated sources. These
 597 have also been added to the table. Where possible, names have been adjusted to be consistent with
 598 the NASA/IPAC Extragalactic Database¹ nomenclature.

599 4.2. Radio searches for pulsars

600 Of the 56 γ -ray emitting pulsars identified in 1FGL, 32 were detected by folding the γ -ray
 601 data using timing solutions from observations of known radio pulsars. These ephemerides have
 602 been collected by a global consortium of radio astronomers who dedicate a portion of their time
 603 toward this effort (Smith et al. 2008). The 32 pulsars (23 young and nine MSPs) had all been
 604 discovered in the radio band prior to their detection by the LAT. Since the release of the 1FGL
 605 catalog, twelve more of the 1FGL sources have been found to have γ -ray pulsations by using
 606 ephemerides of known radio pulsars. While eight of the twelve were associated in 1FGL with a
 607 pulsar or a SNR/PWN, four were listed as unassociated sources in the catalog (two young pulsars
 608 and two MSPs). These new associations are listed in Table 7.

609 In addition to folding data using the properties of known radio pulsars, a promising technique
 610 for identifying unassociated sources is searching for previously unknown radio pulsars that might
 611 be powering the γ -ray emission. This technique was used on many of the EGRET unidentified
 612 sources (Champion et al. 2005; Crawford et al. 2006; Keith et al. 2008, for example) with modest
 613 success, because the error boxes were many times larger than a typical radio telescope beam. With
 614 the LAT, the unassociated source localizations are a much better match to radio telescope beam
 615 widths and generally each can be searched in a single pointing.

¹<http://ned.ipac.caltech.edu/>

616 Thus far, over 450 unassociated LAT sources, mostly at high Galactic latitudes, have been
 617 searched by the *Fermi* Pulsar Search Consortium (PSC; Ransom et al. 2011) at 350, 820, or 1400
 618 MHz. The target lists for these searches were selected from the LAT unassociated sources, with
 619 preference for those that displayed low variability and a spectrum consistent with an exponential
 620 cutoff in the few GeV range, as seen in the identified γ -ray pulsar population (Abdo et al. 2010l).
 621 This program has resulted in the discovery of 32 previously unknown radio pulsars (one young
 622 pulsar and 31 MSPs) (Ray & Parkinson 2011; Keith et al. 2011; Cognard et al. 2011; Bangale et al.
 623 2011) that are included in Table 7. Of these 32 new pulsars, 14 also show pulsations in γ rays.
 624 There is no obvious correlation between the γ -ray and radio fluxes of these pulsars, so additional
 625 discoveries can be expected as fainter unassociated 1FGL sources are searched.

626 Searches by the PSC continue. In the Galactic plane, high dispersion measures and sky tem-
 627 peratures demand higher frequency observations with concomitantly smaller beam sizes. Young,
 628 energetic pulsars can be very faint in the radio (Camilo et al. 2002b,a). Nevertheless, we expect
 629 that deep observations will continue to turn up more discoveries of radio pulsars in unassociated
 630 1FGL sources in the near future.

631 To summarize, radio observations of sources in the 1FGL unassociated sample have produced 36
 632 new pulsar associations. 18 of these pulsars are considered firm identifications due to the detection
 633 of pulsations in the LAT data.

634 4.3. X-ray observations of unassociated source fields

635 To look for additional possible counterparts we cross-correlated the list of unassociated 1FGL
 636 sources with existing X-ray source catalogs. We stress that the resulting compilation has no claim
 637 of completeness since the match with cataloged X-ray sources depends on the serendipitous sky
 638 coverage provided by the X-ray observations, and the integration time of the observation. While
 639 it is possible that candidate X-ray counterparts to the LAT unassociated sources may be singled
 640 out on the basis of, e.g., their brightness and/or spectral properties, most will be recognized only
 641 through a coordinated multiwavelength identification approach (which is beyond the scope of this
 642 paper).

643 To begin, we considered the 2XMM source catalog derived from pointed *XMM*-Newton ob-
 644 servations (Watson et al. 2008). The fourth incremental release of the catalog (2XMMi) includes
 645 191,870 unique X-ray sources extracted from all *XMM*-Newton observations that were public as of
 646 2008 May 1, i.e. performed through the end of 2007 April. We cross-correlated the LAT source lists
 647 with the 2XMMi catalog, using a cross-correlation radius equal to the semi-major axis of the 95%
 648 confidence ellipse of the LAT source, and found that 40 of the 1FGL unassociated fields contained
 649 2XMMi detections. Of these 40, four had been found to be associated with AGN by the radio
 650 follow-up observations (Section 4.1).

651 By looking at the *XMM*-Newton observation log (up to 2011 February 27) we can estimate the

652 potential increase in the number of matches that could occur if we were to use the longer obser-
 653 vational database. For the cross-correlation we used the LAT 95% semi-major axis and compared
 654 against a radius equal to the sum in quadrature of the EPIC camera radius ($15'$) and the r95
 655 positional uncertainty for the X-ray source. Here we found another 17 fields of unassociated LAT
 656 sources that have been observed by *XMM-Newton*, either serendipitously or pointed.

657 In addition, we cross-correlated with the *ROSAT* All Sky Survey Bright and Faint Source
 658 Catalogs (Voges et al. 1999, 2000a) and with the *ROSAT* catalog of pointed Position-Sensitive
 659 Proportional Counter (PSPC) (Voges et al. 1994) and High Resolution Imager (HRI) (Voges et al.
 660 2000b) observations. These found 101 unassociated source fields with ROSAT counterparts, 15 of
 661 which were also found in the 2XMMi correlation. These results are summarized in Table 7, and
 662 show that a preliminary X-ray screening provides potential X-ray counterparts for about 20% of
 663 all the *Fermi*-LAT unassociated sources. These possible X-ray counterparts are obviously prime
 664 targets for multiwavelength follow-up observations.

665 We also compared the 1FGL unassociated source list with recently published catalogs of hard
 666 X-ray/soft γ -ray sources. These are the *Palermo Swift-BAT Hard X-ray Catalog* (Cusumano et al.
 667 2010) which is a compilation of 754 sources detected by the BAT instrument in its first 39 months
 668 of operations, and the 4th *IBIS/SGRI* Soft γ -ray Survey Catalog (Bird et al. 2010) which includes a
 669 total of 723 sources. Both catalogs contain flux and spectral information and provide likely source
 670 identification/classification. We cross-correlated the *Swift*-BAT and *IBIS/SGRI* source catalogs
 671 using the nominal 1FGL position and 95% semi-major axis as before, and found 11 new associations
 672 and 8 new X-ray detections (cases where the candidate X-ray counterpart is not a known γ -ray
 673 emitter). The 1FGL 95% positional error is larger than the positional errors on sources in both
 674 catalogs. These results are also included in Table 7, where we give the *Swift*-BAT and Integral-
 675 *IBIS/SGRI* source identifications and proposed catalog classifications.

676 We note that a preliminary cross-correlation of the LAT unassociated sources with the ROSAT
 677 sources has been performed by Stephen et al. (2010). However, they used only the ROSAT Bright
 678 Source Catalog as a reference and found, on statistical grounds, that 60 of the 77 correlated po-
 679 sitions should be genuine associations. However, they provide likely associations for only 30 of
 680 the correlations, those with counterparts within $160''$. Table 7 lists 26 of these correlated sources.
 681 Three are not listed because the counterpart source type is not a known γ -ray emitter. The final
 682 source is not listed because no counterpart name was provided.

683 A survey of 21 fields of unassociated 1FGL sources was carried out by Mirabal (2009) using
 684 data from the Swift science archive. This investigation indicated X-ray detections for seven LAT
 685 unassociated sources based on positional correlation with Swift-XRT sources and the likelihood the
 686 source is a member of a γ -ray emitting class. Three of these are unique to this investigation and
 687 have been included as X-ray detections. In addition, Mirabal et al. (2010) proposed nine possible
 688 associations for unassociated LAT sources at $|b| > 25^\circ$ in the 3000 square degree “overlap region”,
 689 a region covered by various radio surveys and by the Sloan Digital Sky Survey. Associations and

690 detections from both these investigations are included in Table 7.

691 The unassociated source 1FGL J1958.9+3459 appears to be nearly coincident with the HMXB
 692 Cygnus X-1, which was recently reported as an *AGILE* source (Sabatini et al. 2010). While this
 693 source meets the criteria to claim a positional association, there is no clear evidence that the source
 694 detected by the LAT is Cyg X-1. In addition, the source 1FGL J1045.2–5942 is positionally coin-
 695 cident with the luminous blue variable (LBV) star, Eta Carinae (η Car). While X-ray observations
 696 of η Car show a 5.54 year periodicity, the γ -ray flux remained constant during the most recent
 697 X-ray minimum in 2008 December – 2009 January. However, due to its unusual γ -ray spectrum
 698 this 1FGL source is still believed to be associated with η Car (Abdo et al. 2010b).

699 To date, X-ray observations have led to positional associations with ten AGNs, seven HMXBs,
 700 one SNR and the LBV Eta Carinae. An additional 110 sources have X-ray detections that are
 701 excellent targets for follow-up multiwavelength observations. These associations can be found in
 702 Table 7.

703 4.4. TeV observations of unassociated sources

704 *Fermi*-LAT spectra have been shown to be good predictors of TeV emission, with 55 1FGL
 705 sources having very high energy (VHE) counterparts (Abdo et al. 2009e, 2010i). The energy range
 706 from ~ 50 GeV to ~ 300 GeV is the only range where the LAT data directly overlap with other
 707 instruments.

708 The LAT team has provided recommendations for follow-up observations of a number of hard-
 709 spectrum sources – including unassociated hard-spectrum sources – that may have VHE coun-
 710 terparts. Coordinated follow-up observations in the TeV regime have been useful in identifying
 711 LAT-detected AGNs (see e.g. Abdo et al. 2009e; Mariotti & MAGIC Collaboration 2010). In ad-
 712 dition, LAT sources have been identified as SNRs by comparing the extension in the LAT data to
 713 the VHE emission by using the same procedure as was used for W51C (Abdo et al. 2009d), W44
 714 (Abdo et al. 2010f) and IC443 (Abdo et al. 2010h). This search has yielded two more identified
 715 SNRs, W28 (Abdo et al. 2010c) and W49B (Abdo et al. 2010e). These associations can be found
 716 in Table 7.

717 We cross-checked the 1FGL unassociated source list with the list of TeV sources from TeVCat²
 718 and current publications. We consider a source to be coincident with a LAT source if its extension
 719 overlaps with the 95% confidence ellipse of the LAT source. We find nine TeV sources that are
 720 coincident with 1FGL unassociated sources (Table 8). Note that the 1FGL association process did
 721 not assign an association to a coincident TeV source if that TeV source had no identification in
 722 another waveband. Pismis 22 and W43 are possible (but not confirmed) associations with the TeV

²<http://tevcats.uchicago.edu>

723 source.

724 One source of note is 1FGL J1702.4–4147 which lies on the emission “tail” of the elongated
 725 VHE source, H.E.S.S. J1702–402. The nearby pulsar PSR J1702–4128 lies at the edge of the
 726 TeV γ -ray emission and would provide enough spin-down energy loss to produce the observed VHE
 727 emission via an extremely asymmetric PWN (Aharonian et al. 2008). Hence the pulsar is considered
 728 to be a likely counterpart to the LAT source. To date there has not been a high significance
 729 detection of pulsations in the LAT data. An additional interesting source, 1FGL J1839.1–0543
 730 is positionally coincident with HESS J1841–055, one of the most extended (1 deg in diameter)
 731 H.E.S.S. unidentified sources. Because of the high density of potential counterpart sources in this
 732 low-latitude region, there are multiple possible associations for the VHE source (2 SNRs, 3 high
 733 spin-down PSRs, 1 XRB) (Aharonian et al. 2008). Given its high TeV γ -ray flux, it is considered
 734 a good candidate for LAT detection (Tibolla 2009).

735 4.5. Association of LAT sources using only LAT data

736 A small number of sources have been associated or identified since the release of the 1FGL
 737 catalog by using LAT data alone. Of the 56 pulsars listed in 1FGL, 24 were discovered using blind
 738 frequency searches (Abdo et al. 2009b) for γ -ray pulsations from the bright unassociated sources.
 739 These are typically young pulsars, for which the solid angle of the radio beam is likely to be much
 740 smaller than the γ -ray one (Abdo et al. 2010). As a result of this geometry, many unassociated
 741 sources are likely to be young, radio-quiet pulsars that will never be found in radio searches. Since
 742 the release of the 1FGL catalog, another blind search pulsar, PSR J0734–1559 has been discovered
 743 in an unassociated LAT source. This association has been included in Table 7.

744 One new HMXB has also been detected in the LAT data (Corbet et al. 2011), though in 1FGL
 745 the source was associated with the SNR G284.3–01.8. This is the first of its type to be discovered
 746 in γ rays. These new associations are also included in Table 7.

747 5. Discussion

748 The follow-up multiwavelength associations efforts discussed in Section 4 have resulted in 177
 749 new extragalactic source associations (all AGN), and 52 new Galactic associations (one source has
 750 both a Galactic and extragalactic association). When we compare these new associations with
 751 the expected 1FGL source distributions discussed in Section 2.4, the estimated numbers of sources
 752 that have not yet been associated are reduced to 182 for extragalactic sources and 219 for Galactic
 753 sources.

754 To test the two classification algorithms and to estimate the efficiency for identifying the
 755 different source classes, we compare the results to the new source associations in Section 4, first

756 looking at individual methods, and then the combined results. In addition, we consider how the
 757 results match the $\text{Log}N\text{-Log}S$ analysis.

758 5.1. Validating the classification results from the separate methods

759 We separately compared the results of the Classification Tree analysis and the Logistic Regres-
 760 sion analysis to the new source associations in Section 4. Altogether, the new source associations
 761 include 177 new AGN associations as well as 37 new pulsar associations that are divided into 2
 762 categories: 20 objects for which pulsations have been detected in γ rays (which we will refer to as
 763 “new pulsar detections”) and 17 objects for which pulsations have been detected only in the radio
 764 (which we will refer to as “new pulsar candidates”). We will not use new associations from other
 765 source types (HMXB, PWN, SNRs) for this validation.

766 For AGN, we find that 126 sources are correctly classified as AGN candidates by the CT analysis
 767 (efficiency: 71%), 11 were classified as pulsar candidates (false negative: 6%), while the remaining
 768 40 sources were considered still unclassified (23%). The same comparison for the LR analysis gave
 769 142 sources correctly classified as AGN candidates (efficiency: 80%), 7 sources classified incorrectly
 770 as pulsar candidates (false negative: 4%), while the other 28 sources remained unclassified (16% of
 771 the sample).

772 For pulsars, we noticed a very different performance between new pulsar detections and new
 773 pulsar candidates. For the 20 sources detected as pulsars by the LAT, the CT analysis correctly
 774 classifies 14 pulsars (efficiency: 70%), mis-classifies one source (5%), and leaves the remaining
 775 sources unclassified (25%). The LR analysis correctly classifies 11 pulsars (efficiency: 55%), mis-
 776 classifies one source (5%), and leaves the remaining sources unclassified (40%). On the other hand,
 777 for the new radio pulsar candidates, the CT analysis correctly classifies only 3 objects as pulsars
 778 (efficiency: 18%), mis-classifies 8 objects as AGN (false negative: 47%) and leave the 6 remaining
 779 objects as still unassociated (35% of the new pulsar candidates). The LR analysis correctly classifies
 780 4 pulsar candidates (efficiency: 23.5%), mis-classifies four sources (23.5%), and leaves the remaining
 781 nine sources unclassified (53%).

782 These results are interesting, as the definition of the pulsar fiducial threshold in the LR analysis
 783 appeared that it might over-estimate the pulsar candidates. However, the Logistic Regression
 784 actually has a somewhat poorer success rate for finding new pulsars and pulsar candidates than the
 785 Classification Tree analysis. Looking more closely at the 1FGL properties of the misclassified pulsar
 786 candidates, we found that twelve of the 17 new pulsar candidates have only upper limits for the
 787 300 MeV – 1 GeV band. In contrast, 80% of the new pulsar detections were significantly detected
 788 in this portion of the LAT spectrum. This difference in characteristics for the two pulsar groups
 789 may indicate the need for additional criteria when selecting sources for follow-up observations.

5.2. Validating the results from the combined classifications

790
 791 We can also compare the new associations to the combined classifications defined in Section 3.4.
 792 Of the 214 newly-associated AGN and pulsars from Section 4, 171 sources (151 new AGN, 16 new
 793 pulsar detections, and 4 new pulsar candidates) match the classification given by the combined
 794 analysis, and 26 sources (15 new AGN, 1 new pulsar detection, and 10 new pulsar candidates)
 795 are in direct conflict with the classification source type. This gives an efficiency of 85% for AGN
 796 classification and 80% for classification of new pulsar detections, but only 59% for new pulsar
 797 candidates. 17 of the newly associated sources are unclassified by either method, and only one
 798 source has conflicting source classification. The one conflicting source turns out to be a new pulsar
 799 candidate that also has an AGN association, suggesting the LAT source could be the sum of these
 800 two objects. The overall efficiency for this combined sample is $\sim 80\%$, comparable to the value we
 801 were seeking when we set the fiducial values for the two methods. The combined sample has a false
 802 negative rate of $\sim 12\%$.

803 The spatial distributions of the newly classified sources give us the opportunity to cross check
 804 our results. Figure 11 shows the spatial distribution of all the sources. Notice that both the AGN
 805 and pulsar distributions are as expected, even though we have not used the Galactic latitude as
 806 an input to either classification method. The pulsar candidates are mainly distributed along the
 807 Galactic plane, with a few high-latitude exceptions that suggest additional nearby MSPs, while the
 808 AGN candidates are nearly isotropically distributed on the sky.

809 From this we can conclude that using only the γ -ray properties of the *Fermi* LAT sources,
 810 and the firm associations of the 1FGL, we were able to develop a prediction for AGN and pulsars
 811 classification that nearly matches our expectations (i.e. pulsar candidates are not variable, have a
 812 curved spectrum and are mainly distributed along the Galactic plane, while AGN candidates are
 813 mostly extragalactic, variable sources). In all, the efficiency of the combined classification methods
 814 at classifying new AGNs is high, with a low rate of false negatives, while the efficiency for new
 815 pulsar candidates is much lower than expected.

816 AGN and pulsars are not the only γ -ray source classes known or expected, but the less-populous
 817 source types are hard to classify using the techniques described here because the training samples
 818 are too small in 1FGL. With time, those training samples will likely grow, and we may be able to
 819 extend this analysis to additional classifications.

5.3. Comparison to the Log N -Log S predictions

820
 821 In addition, we can check to see how the classification results compare to the predictions made
 822 by the Log N -Log S analysis in Section 2.4. For this comparison, we consider a pulsar classification
 823 to be indicative of a Galactic source, and an AGN classification to be indicative of an extragalactic
 824 source.

825 Since 229 of the unassociated sources now have associations, we will consider only those 401
 826 that remain unassociated. Thirty-three of these are unclassified by either technique, and 13 have
 827 conflicting classifications. The number sources for low latitudes and high latitudes for the remaining
 828 355 are shown in Table 2. At high latitudes, the observed numbers of both Galactic and extragalac-
 829 tic sources are consistent with the numbers expected from the $\text{Log}N\text{-Log}S$ analysis. In contrast,
 830 at low latitudes, the number of Galactic sources is about one-third lower than expected, and the
 831 number of extragalactic sources is higher than expected. It is clear that the group of sources that
 832 is hardest to associate is those of Galactic origin at low latitudes, likely due to the presence of a
 833 population of spurious sources in that region in the 1FGL catalog.

834 Figure 12 (left panel) shows the latitude distribution of the classified unassociated sources
 835 based on classification type. If we combine the AGN candidate population with the 1FGL sources
 836 that already have AGN associations (Figure 12, right panel), we find that the shape of the AGN
 837 distribution matches reasonably with that predicted by the model, though there is still an excess
 838 at low Galactic latitudes.

839 5.4. Unassociated sources at low Galactic latitudes

840 It is the unassociated sources in the central 20° of Galactic latitude ($|b| < 10^\circ$) that may hold
 841 clues to the content of the narrow Galactic ridge population at $|b| < 0.5^\circ$, $|l| < 60^\circ$ discussed in
 842 Section 2.1. To investigate these sources, we separate the pulsar candidates from the other types
 843 of sources (Figure 13) and consider the distribution. Where the full set of unassociated sources
 844 appears to indicate an unreasonably narrow scale height of ~ 50 pc for the population, the latitude
 845 distribution of pulsar candidates is somewhat closer to expectations, implying a scale height of ~ 85
 846 pc. This value is one-third the scale height of LAT-detected γ -ray pulsars (Abdo et al. 2010l).

847 For γ -ray sources, this population scale height suggests instead that Population I objects such
 848 as SNRs, with a scale height of ~ 100 pc (Lamb & Macomb 1997), are likely significant contributors
 849 to the 1FGL sources. In the 1FGL catalog, 44 sources were associated with or identified as SNRs,
 850 and this paper associates six more (Table 7), giving a total of 50 SNR associations. Considering
 851 that only 63 1FGL sources were associated/identified with pulsars, it is clear that both source types
 852 are significant contributors. The classification method used here does not consistently label SNRs
 853 as pulsar candidates. Of the six new SNR associations, five are classified as pulsar candidates, and
 854 the sixth is classified as an AGN. In the future it may be useful to consider the SNR source class
 855 separately as an input to such classification analyses.

856 This central portion of the Galaxy is also the region that has most of the sources that are
 857 either unclassified or have conflicting classifications. Of the 257 unassociated sources in this region,
 858 22 have no classification, and 29 have conflicting classifications between the two methods. Of these
 859 51 unclassified or conflicting-classification sources, eight have new associations. The source types
 860 are varied; two MSPs, one young pulsar, three HMXBs and two AGN. It is clear that not all of

861 these sources can be spurious, however it is unlikely the remaining 43 are all real detections.

862

5.5. Informing future follow-up observations

863 The results of the classification analyses demonstrate that source properties measured with
 864 the *Fermi*-LAT can provide important guidance on what types of follow-up observations are likely
 865 to be fruitful for many of these unassociated sources. The emphasis in follow-up observations of
 866 LAT sources has been on radio imaging and timing observations for a large number of sources,
 867 as well as targeted X-ray observations for sources of interest (e.g. flaring sources or new radio
 868 pulsar candidates). In addition, there is an on-going program to observe all the bright, well-
 869 localized *Fermi*-LAT unassociated sources with *Swift*³ that may add important new insights into
 870 these sources as a group.

871 In Table 4, the last 4 columns show what follow-up observations are recommended in several
 872 wavebands. Obviously, sources classified as likely blazars would benefit from radio searches for
 873 flat-spectrum sources within the LAT error ellipse. Low-frequency radio timing is recommended
 874 for the likely pulsars. X-ray observations of likely pulsars can give timing observers seed locations
 875 at which to search for pulsations in both radio and LAT data (Caraveo 2009). Still-unassociated
 876 sources that may benefit from such observations have been flagged in the 1FGL unassociated source
 877 list with the appropriate observation type. These are suggestions; it is highly likely that some of
 878 the sources are misclassified. Also, a number of the follow-up observations discussed here have
 879 yielded no new associations for some of the observed unassociated sources.

880 We strongly recommend additional joint analyses of LAT and ground-based VHE γ -ray data
 881 for very low-latitude ($|b| < 0^\circ.5$) *Fermi* sources. Together, these may give insight into whether or
 882 not a population of SNRs can account for a significant number of the 1FGL unassociated sources
 883 along the Galactic ridge. Sources for which this type of analysis is recommended are indicated in
 884 the 1FGL unassociated source list (Table 4).

885

5.6. Remaining BSL unassociated sources

886 Follow-up observations like those discussed in the previous section have made a significant
 887 impact, increasing the associated fraction for the 1FGL catalog from $\sim 56.5\%$ to $\sim 71\%$ in only a
 888 little more than one year. But we can look farther back to the *Fermi*-LAT Bright Source List (BSL
 889 Abdo et al. 2009f), the list of 205 high significance ($> 10\sigma$) LAT sources detected in the first three
 890 months of the *Fermi* mission. Of the 37 sources listed as unassociated in the BSL, ten now have
 891 pulsar identifications or associations, while eight have new AGN associations. In addition, seven

³<http://www.swift.psu.edu/unassociated/>

892 have been associated with other γ -ray source types such as SNRs or HMXBs. These associations
 893 bring the BSL association rate up to 94%.

894 Of the remaining twelve BSL unassociated sources, five lie in the Galactic ridge and should be
 895 considered with caution. Here we look more closely at these 12 sources:

- 896 • **1FGL J0910.4–5055** (0FGL J0910.2–5044) – This Galactic plane transient ($l, b = 271^\circ.7, -1^\circ.96$)
 897 flared once in October 2008, an event lasting 1–2 days with peak flux ($E > 100$ MeV)
 898 of 1×10^{-6} ph cm $^{-2}$ s $^{-1}$ (Cheung et al. 2008). (1FGL reported a peak flux for this source
 899 of 1.97×10^{-7} ph cm $^{-2}$ s $^{-1}$, but that was averaged over one month.) Recent figure-of-merit
 900 analysis by Murphy et al. (2010) has given this source a $> 80\%$ probability of being associated
 901 with the radio source AT20G J091058-504807. Our analysis does not find such an association,
 902 though Mirabal (2009) does show an association with the likely blazar *Swift* J0910.9–5048.
- 903 • **1FGL J1311.7–3429** (0FGL J1311.9–3419) – Besides being associated with 3EG J1314–3431,
 904 this very bright high-Galactic latitude ($l, b = 307^\circ.7, 28^\circ.2$) source is not variable and has a
 905 spectrum with a high-energy cutoff very similar to a pulsar. To date, searches for both γ -ray
 906 and radio pulsations from this source have been unsuccessful (Ransom et al. 2011).
- 907 • **1FGL J1536.5–4949** (0FGL J1536.7–4947) – With no significant variability, this persis-
 908 tently bright mid-latitude ($l, b = 328^\circ.2, 4^\circ.8$) source is the only unassociated BSL source to
 909 have conflicting classifications. This source has a moderately curved spectrum with a high-
 910 energy cutoff.
- 911 • **1FGL J1620.8–4928c** (0FGL J1622.4–4945) – This moderately bright source in the Galac-
 912 tic ridge ($l, b = 333^\circ.9, 0^\circ.4$) is spatially coincident with the *AGILE* detection 1AGL J1624-4946,
 913 and has a spectrum with a sharp spectral break at ~ 3 GeV. There is no evidence at this
 914 time for pulsations from this source in either γ rays or radio (Ransom et al. 2011).
- 915 • **1FGL J1653.6–0158** (0FGL J1653.4–0200) – Another non-varying source with a pulsar-like
 916 spectrum, this high-latitude ($l, b = 16^\circ.6, 24^\circ.9$) source is associated with 3EG J1652–0223.
 917 Both classification methods call this source a pulsar candidate.
- 918 • **1FGL J1740.3–3053c** (0FGL J1741.4–3046) – The position for this non-varying c-source
 919 in the Galactic ridge ($l, b = 357^\circ.7, -0^\circ.1$) moved far enough between the two publications
 920 that the two detections are not formally associated. However, we recall that for pulsars in
 921 the plane, the 1FGL error ellipse appears to underreport the systematic error. As the BSL
 922 source lies just outside the 1FGL 95% confidence contour, we consider the two detections to
 923 be related.
- 924 • **1FGL J1839.1–0543c** (0FGL J1839.0–0549) – This bright source in the Galactic ridge
 925 ($l, b = 26^\circ.4, 0^\circ.1$) has a highly curved spectrum and does not vary. Both classification methods
 926 call this source a pulsar candidate.

- 927 • **1FGL J1842.9–0359c** (0FGL J1844.1–0335) – This Galactic ridge source ($l, b = 28^\circ 4, 0^\circ 1$)
 928 had a source significance of 10σ in the first three months, but after eleven months that
 929 value has increased only slightly, to 10.9σ (unless variable, a source should have twice the
 930 significance after nearly four times the livetime). Since 1FGL found this source to be non-
 931 varying, it is unlikely that the low flux in 1FGL is due to variability effects. Instead, it appears
 932 that the longer data set has separated the BSL source into multiple components, leaving the
 933 coincident 1FGL source at a lower-than-expected significance.

- 934 • **1FGL J1848.1–0145c** (0FGL J1848.6–0138) – Another source in the Galactic ridge ($l, b =$
 935 $31^\circ 0, -0^\circ 1$), its spectrum is consistent with a power-law, and the source may be related to a
 936 TeV source (see Table 8).

- 937 • **1FGL J2027.6+3335** (0FGL J2027.5+3334) – A bright, mildly variable source that lies
 938 near the Galactic plane ($l, b = 73^\circ 3, -2^\circ 9$), this source is associated with the EGRET source
 939 3EG J2027+3429. In the 1FGL catalog, this source flux peaked at 3.4×10^{-7} ph cm $^{-2}$ s $^{-1}$ with
 940 a significance $> 10\sigma$ in a single month. The spectrum has a large curvature index, indicating
 941 that it is not a simple power-law. Although the variability seems to indicate a possible AGN,
 942 both classification methods consider it a likely pulsar.

- 943 • **1FGL J2111.3+4607** (0FGL J2110.8+4608) – While this source near the Galactic plane
 944 ($l, b = 88^\circ 3, -1^\circ 4$) is highly significant, it is flagged in the 1FGL catalog as having the flux
 945 measurement that is sensitive to changes in the diffuse model. Even so, the spectrum is
 946 moderately pulsar-like with a high-energy cutoff and there is no hint of variability. Both
 947 classification techniques consider this source a pulsar candidate.

- 948 • **1FGL J2339.7–0531** (0FGL J2339.8–0530) – This very hard source (spectral index = 1.99)
 949 lies at high Galactic latitude ($l, b = 81^\circ 4, -62^\circ 5$). While its 1FGL five-band spectrum suggests
 950 a blazar, neither classification method was able to classify this source.

951 While five of these are c-sources, only two (1FGL J1842.9–0359c and 1FGL J1848.1–0145c)
 952 appear to be questionable, though the possibility of a TeV component for the latter should be
 953 investigated. The two variable sources seem likely to be AGN. The γ -ray characteristics of the
 954 majority of the other unassociated BSL sources imply that these sources are bright, steady, and
 955 have curved spectra with high-energy cutoffs. With the exception of 1FGL J0910.4–5055, all these
 956 sources were included in the searches for radio pulsations, the same searches which have resulted in
 957 the discovery of ten new MSPs in unassociated BSL sources. Blind searches for pulsations in the
 958 γ -ray data have also been performed on these sources, with no success.

959 One source of interest is 1FGL 2017.3+0603, a BSL source that now has detected pulsations
 960 in the LAT data (Cognard et al. 2011) as well as an AGN association with a high figure of merit
 961 (0.923) in 1LAC (Abdo et al. 2010k). This source will require additional analysis to determine if
 962 the LAT flux is due solely to the pulsar, or is a combination of both counterparts.

5.7. Comparing with EGRET unassociated sources

963

964 Although the present paper is focused on the *Fermi*-LAT unassociated sources, some insight
 965 about these sources may be found from the all-sky survey with EGRET on the *Compton Gamma*
 966 *Ray Observatory*. Using the LAT results, with higher sensitivity and better source locations, as
 967 a reference, we re-examine the sources of two EGRET catalogs: the 3EG catalog (Hartman et al.
 968 1999) and the EGR catalog (Casandjian & Grenier 2008). The two catalogs were based largely on
 969 the same data, while they used different models of the diffuse γ radiation that forms a background
 970 for all sources. In addition, noting those EGRET unassociated sources that remain unassociated
 971 in the 1FGL catalog offers the opportunity to recognize sources that remain interesting on a time
 972 scale of decades.

973

5.7.1. Experience with the EGRET Catalogs

974 A comparison of the two EGRET catalogs with each other and with the LAT 1FGL catalog
 975 yields several observations and tentative conclusions, illustrated by specific examples. Because
 976 more detailed information is available about the 3EG sources, many of these results emphasize that
 977 catalog, although similar considerations likely apply to the EGR analysis.

978

979

980

981

982

983

984

985

986

987

1. The statistical error contours produced for EGRET underestimated the full uncertainty in the source localization. The Crab, Vela, Geminga, and PSR J1709–4429 pulsars, which are positively identified by γ -ray pulsations in both EGRET and *Fermi*-LAT data, have positions outside the formal error contours, even at the 99% level, as noted by Hartman et al. (1999). For 3EG, but not for EGR, the CTA 1 and LSI +61° 303 sources, now firmly identified by LAT, also lie outside the 95% error contours. For this reason, we expand the list of plausible associations to include all those LAT sources whose position falls within the 99% error contours. As noted by Hartman et al. (1999), however, the EGRET source localizations were better at higher Galactic latitudes. Even bright AGN such as 3C279 were typically found within the error contours.

988

989

990

991

992

993

994

995

2. The circular fit to the EGRET 95% error contour was a poor approximation in many cases. In addition to the 107 matches between 1FGL and 3EG reported based on the automated comparison using this circular fit, there are 21 more 1FGL sources found within the 95% error contours of the detailed 3EG uncertainty contour maps (Hartman et al. 1999). Further, 19 1FGL sources are located between the 3EG 95% and 99% contours, making a total of 149 candidate associations, or 153 including the four bright pulsars identified by timing. The 14 other 1FGL sources that lie just outside the 3EG 99% contours are not included in this analysis, although they remain potential association.

996

997

3. The adopted diffuse background model is important both close to and far from the Galactic plane. For example, EGR J0028+0457 is confirmed by the LAT as the millisecond pulsar PSR

998 J0030+0451 (Abdo et al. 2009h) at a Galactic latitude of -57° . There was no correspond-
999 ing source in the 3EG catalog, though a sub-threshold excess was seen (Thompson 2010).
1000 Conversely, 3EG J1027–5817, at a Galactic latitude of -1° is confirmed by the LAT as PSR
1001 J1028–5819 (Abdo et al. 2009c), while the nearest EGR source is nearly 1° away with a 95%
1002 error uncertainty of 0.22° .

- 1003 4. Variability is an important consideration even for sources not associated with blazars. The
1004 EGRET upper limit for radio galaxy NGC 1275, derived from Figure 3 of Hartman et al.
1005 (1999), lies nearly an order of magnitude below the LAT detection level (Kataoka et al.
1006 2010). 3EG J0516+2320 was a bright solar flare from 1991 June (Kanbach et al. 1993). The
1007 1FGL catalog contains no solar flares. 3EG J1837–0423 (Tavani et al. 1997) was one of the
1008 brightest sources in the γ -ray sky in 1995 June, at a flux ($E > 100$ MeV) of $(3.1 \pm 0.6) \times 10^{-6}$
1009 $\text{ph cm}^{-2} \text{s}^{-1}$. No 1FGL source is seen consistent in position with this source, even though
1010 the LAT would have detected a source nearly 2 orders of magnitude fainter (see Figure 19 of
1011 Abdo et al. 2010a).

1012 Some of these lessons from the EGRET era have already been applied to the 1FGL catalog
1013 construction but are worth reiterating in any discussion of unassociated sources.

- 1014 1. Unlike EGRET, the error contours for 1FGL include a systematic component of 10% added
1015 to the statistical uncertainties. This component was derived, however, from high-latitude
1016 AGN comparisons. The EGRET experience suggests that the situation will be more difficult
1017 at lower Galactic latitudes. The low-latitude LAT source associated with LS5039 based on
1018 periodicity, for example, has a measured position that lies at the 95% uncertainty contour
1019 even after adding a 20% systematic component (Abdo et al. 2009g). This is an additional
1020 indication that the LAT positional uncertainties for sources in the Galactic plane are affected
1021 by the systematics discussed earlier.
- 1022 2. Even without any additional systematic uncertainty, it should be remembered that at least
1023 5%, or more than 70, of the 1FGL sources probably have true counterparts that fall outside
1024 the 95% contours.
- 1025 3. Just as the EGRET catalog used “C” for potentially confused regions and “em” for possibly
1026 extended or multiple sources, the 1FGL catalog identifies sources with a “c” in the name or a
1027 numerical flag to indicate possible uncertainties due to the analysis procedure or the diffuse
1028 model. The LAT has confirmed $\sim 67\%$ of EGRET sources that do not carry either the “C”
1029 or “em” flags, but has only confirmed $\sim 38\%$ of the flagged sources. This experience with
1030 EGRET certainly suggests that such flags should be taken seriously.

5.7.2. 1FGL Unassociated Sources Remaining from the EGRET Era

1031

1032 Despite the gap of more than a decade between the EGRET and LAT observations, a sizable
 1033 number of the unassociated sources seen by EGRET are associated with 1FGL sources that are
 1034 unassociated with known source classes. Whether they are persistent or recurrent, such sources
 1035 offer a high potential for multiwavelength studies. Table 7 includes 43 positional coincidences we
 1036 have found between unassociated sources in the EGRET and 1FGL catalogs. As noted above,
 1037 the predominance of 3EG sources results at least partly from the additional information available
 1038 compared to the EGR catalog, which did not include confidence contour maps.

1039

1040 These unassociated sources are distributed widely across the sky. Only 10 of the 43 have “c”
 1041 designations in 1FGL, and all of these lie close to the Galactic plane toward the inner Galaxy,
 1042 where the Galactic diffuse emission is brightest and any deficiencies in the model of the diffuse
 1043 emission would have the greatest effect on properties of the 1FGL sources. Although the EGRET
 1044 localization uncertainties are large, the density of 1FGL sources away from the Galactic Plane
 1045 is not so large that accidental coincidences are a significant problem. EGR J1642+3940 (1FGL
 1046 J1642.5+3947) appears to be a special case. It appeared in the EGRET data only after the end
 1047 of the 3EG data set, but it has been seen by the LAT. Casandjian & Grenier (2008) suggest an
 1048 association with blazar 3C 345, although it might also be associated with Mkn 501 (Kataoka et al.
 1049 1999). Although it is shown as unassociated in the 1FGL catalog, recent LAT analysis also suggests
 one or more blazars contribute to this source (Schinzel et al. 2010).

1050

6. Conclusions

1051

1052 As the *Fermi* mission matures, it is important to take a look at the successes of the early
 1053 mission to help inform and improve the association and follow-up of new sources. The continued
 1054 multiwavelength observations and ongoing statistical association efforts for the 1FGL unassociated
 1055 sources have led to associations for 70% of the entire catalog. Since the release of the catalog, 45%
 1056 of all the extragalactic sources expected from the Log N -Log S analysis have been associated. In
 1057 addition, 47% of the expected high-latitude Galactic sources have been associated. Together, this
 1058 gives associations for nearly 82% of all expected extragalactic and nearly 62% of expected high-
 1059 latitude Galactic sources. However, there are associations for only $\sim 38\%$ of the expected sources
 of Galactic origin that lie at $|b| < 10^\circ$.

1060

1061 The significant improvement in sensitivity of the *Fermi*-LAT relative to EGRET, the sub-
 1062 stantially improved positional errors, and the sky-survey viewing plan made possible by the large
 1063 field of view of the LAT have generated an unprecedented data set and allowed the production
 1064 of the deepest-ever catalog of the GeV sky. From that foundation, the astronomical community
 1065 has worked in concert to discover new additions to known γ -ray source classes, as well as adding
 1066 SNRs, PWNe, starburst galaxies, radio galaxies, HMXBs, globular clusters and a treasure trove of
 millisecond pulsars to the list.

1067 With that success as a backdrop, there are clearly lessons we have learned from the 1FGL
1068 catalog process and follow-up analyses, as well as from experience with previous missions:

- 1069 1. As discussed in Abdo et al. (2010a), it is clear that there is room for improvement in the plane
1070 of the Galaxy, and especially the ridge. This region contributes numerous questionable sources
1071 to the catalog. However, if we set that region aside, essentially half of the remaining 1FGL
1072 unassociated sources in other regions now have associations, giving an overall association rate
1073 of $\sim 70\%$ for 1FGL. In contrast, the 3rd EGRET catalog had an association rate of only 38%.
- 1074 2. Follow-up campaigns to associate or identify the LAT-detected sources have been extremely
1075 successful. A total of 178 new blazar candidate associations have been made, primarily by
1076 looking for radio candidates within the LAT error ellipses and then re-observing at additional
1077 frequencies to determine if the source has the characteristic flat spectrum in the radio. Thirty-
1078 one new Galactic field MSPs have been discovered based on locations provided by the LAT
1079 for radio pulsations searches.
- 1080 3. By using the distribution of detected sources, we can model the 1FGL γ -ray sky and predict
1081 how many of each general source type we expect in the catalog. After taking into account the
1082 associations made since the release of the 1FGL catalog, this analysis indicates that, as the
1083 mission continues, we might expect to find associations for at least ~ 200 more AGN (mostly
1084 at high Galactic latitudes) and ~ 50 new pulsars (equally divided at high and low latitudes)
1085 among the unassociated 1FGL sources.
- 1086 4. We have applied two analysis techniques to infer the likely classification for unassociated
1087 sources, based solely on their γ -ray properties. The γ -ray properties of sources, while not
1088 being sufficient on their own to determine source type, can provide important information
1089 regarding the parent source classes. Using the information provided by the LAT to inform
1090 the selection of γ -ray sources and wavelengths for follow-up studies can reduce the labor
1091 intensive nature of such observations and increase the likelihood of finding a viable association
1092 candidate. A preliminary assessment of this process shows a success rate of $\sim 80\%$.

1093

7. Acknowledgments

1094 The *Fermi* LAT Collaboration acknowledges generous ongoing support from a number of
1095 agencies and institutes that have supported both the development and the operation of the LAT as
1096 well as scientific data analysis. These include the National Aeronautics and Space Administration
1097 and the Department of Energy in the United States, the Commissariat à l’Energie Atomique and
1098 the Centre National de la Recherche Scientifique / Institut National de Physique Nucléaire et de
1099 Physique des Particules in France, the Agenzia Spaziale Italiana and the Istituto Nazionale di Fisica
1100 Nucleare in Italy, the Ministry of Education, Culture, Sports, Science and Technology (MEXT),

1101 High Energy Accelerator Research Organization (KEK) and Japan Aerospace Exploration Agency
1102 (JAXA) in Japan, and the K. A. Wallenberg Foundation, the Swedish Research Council and the
1103 Swedish National Space Board in Sweden.

1104 Additional support for science analysis during the operations phase is gratefully acknowledged
1105 from the Istituto Nazionale di Astrofisica in Italy and the Centre National d’Études Spatiales in
1106 France.

1107 *Facilities: Fermi-LAT.*

1108 REFERENCES

1109 Abdo, A. A., et al. 2009a, ApJ, 700, 597

1110 —. 2009b, Science, 325, 840, (Blind Search Pulsars)

1111 —. 2009c, ApJ, 695, L72, (PSR J1028–5819)

1112 —. 2009d, ApJ, 706, L1

1113 —. 2009e, ApJ, 707, 1310

1114 —. 2009f, ApJS, 183, 46, (Bright Source List)

1115 —. 2009g, ApJ, 706, L56, (LS5039)

1116 —. 2009h, ApJ, 699, 1171, (PSR J0030+0451)

1117 —. 2010a, ApJS, 188, 405, (1FGL Catalog)

1118 —. 2010b, ApJ, 723, 649

1119 —. 2010c, ApJ, 718, 348

1120 —. 2010d, ApJ, 719, 1433

1121 —. 2010e, ApJ, 722, 1303

1122 —. 2010f, Science, 327, 1103

1123 —. 2010g, ApJ, 722, 520

1124 —. 2010h, ApJ, 712, 459

1125 —. 2010i, ApJ, 711, 64

1126 —. 2010j, ApJ, 720, 435

1127 —. 2010k, ApJ, 715, 429

- 1128 —. 2010l, *ApJS*, 187, 460
- 1129 —. 2011a, *ApJ*, in press - HESS J1825–137
- 1130 —. 2011b, *ApJS*, (2FGL Catalog, in preparation)
- 1131 —. 2011c, *Science*, 331, 739
- 1132 Ackermann, M., et al. 2010, *ApJ*, 721, 1383
- 1133 —. 2011, *ApJ*, 726, 35
- 1134 Aharonian, F., et al. 2006, *ApJ*, 636, 777
- 1135 —. 2008, *A&A*, 477, 353
- 1136 Atwood, W. B., et al. 2009, *ApJ*, 697, 1071, (LAT)
- 1137 Bangale, P., et al. 2011, *ApJ*, in preparation
- 1138 Bird, A. J., et al. 2010, *VizieR Online Data Catalog*, 218, 60001
- 1139 Bock, D., Large, M. I., & Sadler, E. M. 1999, *AJ*, 117, 1578
- 1140 Breiman, L., Freidman, J. H., Olshen, R. A., & Stone, C. J. 1984, *Classification and Regression*
1141 *Trees* (Monterey, CA: Wadsworth and Brooks), new edition
- 1142 Browne, I. W. A., et al. 2003, *MNRAS*, 341, 13
- 1143 Brun, R., & Rademakers, F. 1997, *Nucl. Instrum. Meth.*, A389, 81
- 1144 Camilo, F., Lorimer, D. R., Bhat, N. D. R., Gotthelf, E. V., Halpern, J. P., Wang, Q. D., Lu, F. J.,
1145 & Mirabal, N. 2002a, *ApJ*, 574, L71
- 1146 Camilo, F., et al. 2002b, *ApJ*, 571, L41
- 1147 Caraveo, P. A. 2009, *ArXiv e-prints*, 0912.4857
- 1148 Casandjian, J.-M., & Grenier, I. A. 2008, *A&A*, 489, 849
- 1149 Castro, D., & Slane, P. 2010, *ApJ*, 717, 372
- 1150 Champion, D. J., McLaughlin, M. A., & Lorimer, D. R. 2005, *MNRAS*, 364, 1011
- 1151 Cheung, C. C., Reyes, L., Longo, F., & Iafate, G. 2008, *The Astronomer’s Telegram*, 1788, 1
- 1152 Cognard, I., et al. 2011, *ApJ*, 732, 47
- 1153 Condon, J. J., Cotton, W. D., Greisen, E. W., Yin, Q. F., Perley, R. A., Taylor, G. B., & Broderick,
1154 J. J. 1998, *AJ*, 115, 1693

- 1155 Corbet, R. H. D., et al. 2011, *The Astronomer’s Telegram*, 3221, 1
- 1156 Crawford, F., Roberts, M. S. E., Hessels, J. W. T., Ransom, S. M., Livingstone, M., Tam, C. R.,
1157 & Kaspi, V. M. 2006, *ApJ*, 652, 1499
- 1158 Cusumano, G., et al. 2010, in *Bulletin of the American Astronomical Society*, Vol. 41, *Bulletin of*
1159 *the American Astronomical Society*, 715
- 1160 Drlica-Wagner, A., & Charles, E. 2011, *ArXiv e-prints*, 1111.2352
- 1161 Ghirlanda, G., Ghisellini, G., Tavecchio, F., & Foschini, L. 2010, *MNRAS*, 407, 791
- 1162 Hartman, R. C., et al. 1999, *ApJS*, 123, 79
- 1163 Healey, S. E., Fuhrmann, L., Taylor, G. B., Romani, R. W., & Readhead, A. C. S. 2009, *AJ*, 138,
1164 1032
- 1165 Healey, S. E., Romani, R. W., Taylor, G. B., Sadler, E. M., Ricci, R., Murphy, T., Ulvestad, J. S.,
1166 & Winn, J. N. 2007, *ApJS*, 171, 61
- 1167 Hocker, A., et al. 2007, *PoS, ACAT*, 040
- 1168 Hoppe, S. 2008, in *International Cosmic Ray Conference*, Vol. 2, *International Cosmic Ray Con-*
1169 *ference*, 579–582
- 1170 Hosmer, D., & Lemeshow, S. 2000, *Applied Logistic Regression*, 2nd edn. (John Wiley & Sons,
1171 Inc., New York)
- 1172 Kanbach, G., et al. 1993, *A&AS*, 97, 349
- 1173 Kataoka, J., et al. 1999, *Astroparticle Physics*, 11, 149
- 1174 —. 2010, *ApJ*, 715, 554
- 1175 Keith, M. J., Johnston, S., Kramer, M., Weltevrede, P., Watters, K. P., & Stappers, B. W. 2008,
1176 *MNRAS*, 389, 1881
- 1177 Keith, M. J., et al. 2011, *MNRAS*, 379
- 1178 Lamb, R. C., & Macomb, D. J. 1997, *ApJ*, 488, 872
- 1179 Mahony, E. K., Sadler, E. M., Murphy, T., Ekers, R. D., Edwards, P. G., & Massardi, M. 2010,
1180 *ApJ*, 718, 587
- 1181 Mariotti, M., & MAGIC Collaboration. 2010, *The Astronomer’s Telegram*, 2916, 1
- 1182 Mattox, J. R., et al. 1996, *ApJ*, 461, 396
- 1183 Mirabal, N. 2009, *ArXiv e-prints*, 0908.1389

- 1184 Mirabal, N., Nieto, D., & Pardo, S. 2010, ArXiv e-prints, 1007.2644
- 1185 Murphy, T., et al. 2010, MNRAS, 402, 2403
- 1186 Myers, S. T., et al. 2003, MNRAS, 341, 1
- 1187 Ong, R. A., VERITAS Collaboration, Paneque, D., & Fermi Large Area Telescope. 2010, The
1188 Astronomer’s Telegram, 2486, 1
- 1189 Perlich, C., Provost, F., & Simonoff, J. S. 2003, J. Mach. Learn. Res., 4, 211
- 1190 Ransom, S. M., et al. 2011, ApJ, 727, L16+
- 1191 Ray, P. S., & Parkinson, P. M. S. 2011, in High-Energy Emission from Pulsars and their Systems,
1192 ed. D. F. Torres & N. Rea, 37
- 1193 Renaud, M., Goret, P., & Chaves, R. C. G. 2008, in American Institute of Physics Conference
1194 Series, Vol. 1085, American Institute of Physics Conference Series, ed. F. A. Aharonian,
1195 W. Hofmann, & F. Rieger, 281–284
- 1196 Sabatini, S., et al. 2010, The Astronomer’s Telegram, 2715, 1
- 1197 Schinzel, F. K., Lobanov, A. P., Jorstad, S. G., Marscher, A. P., Taylor, G. B., & Zensus, J. A.
1198 2010, ArXiv e-prints, 1012.2820
- 1199 Smith, D. A., et al. 2008, A&A, 492, 923
- 1200 Stephen, J. B., Bassani, L., Landi, R., Malizia, A., Sguera, V., Bazzano, A., & Masetti, N. 2010,
1201 MNRAS, 408, 422
- 1202 Swanenburg, B. N., et al. 1981, ApJ, 243, L69
- 1203 Tavani, M., et al. 1997, in American Institute of Physics Conference Series, Vol. 410, Proceedings
1204 of the Fourth Compton Symposium, ed. C. D. Dermer, M. S. Strickman, & J. D. Kurfess,
1205 1253–1256
- 1206 Tavani, M., et al. 2011, Science, 331, 736
- 1207 Thompson, D. J. 2010, personal communication
- 1208 Thompson, D. J., et al. 1993, ApJS, 86, 629
- 1209 Tibolla, O. 2009, in American Institute of Physics Conference Series, Vol. 1112, American Institute
1210 of Physics Conference Series, ed. D. Bastieri & R. Rando, 211–222
- 1211 Tibolla, O., et al. 2009, ArXiv e-prints, 0912.3811
- 1212 Vandenbroucke, J., et al. 2010, ApJ, 718, L166

- 1213 Voges, W., Gruber, R., Haberl, F., Kuerster, M., Pietsch, W., & Zimmermann, H. U. 1994, VizieR
1214 Online Data Catalog, 9010, 0
- 1215 Voges, W., et al. 1999, VizieR Online Data Catalog, 9010, 0
- 1216 —. 2000a, VizieR Online Data Catalog, 9029, 0
- 1217 —. 2000b, VizieR Online Data Catalog, 9029, 0
- 1218 Watson, M. G., et al. 2008, VizieR Online Data Catalog, 349, 30339

Table 1. Spatial distribution of various source associations from the 1FGL and 1LAC catalogs

Source class	Sources at $ b > 10^\circ$	Sources at $ b < 10^\circ$	Ridge ^a sources
Associated	670	151	31
AGN	642	51	1
Pulsars	16	47	11
SNRs/PWNe	1	45	19
Other	11	8	0
Unassociated	373	257	88
Non-c sources	354	139	0
c-sources	19	118	88

^aHere, the Galactic ridge is defined as sources with $|b| < 1^\circ$ and $|l| < 60^\circ$. This value is a subset of the previous column of $|b| < 10^\circ$ sources.

Table 2. Expected vs. Observed source distribution

Source types	Sources at $ b > 10^\circ$	Sources at $ b < 10^\circ$	Totals
Total detected	1043 (71.9%)	408 (28.1%)	1451
Associated	670	151	821
Unassociated	373	257	630
Extragalactic			
Total from LogN-LogS	972	88	1060 (73.1%)
Associated	650	51	701
Not Associated in 1FGL	322	37	359
New Associations	150	27	177
New Classifications	154	67	221
LogN-LogS Comparison	-18	+57	+39
Galactic			
Total from LogN-LogS	71	320	391 (26.9%)
Associated	20	100	120
Not Associated in 1FGL	51	220	271
New Associations	27	25	52
New Classifications	31	103	134
LogN-LogS Comparison	+7	-92	-85

Note. — Results from LogN-LogS analysis, applied to the 1FGL source list.

Table 3. Ranking of the training variables for the Classification Tree.

Variable	Importance
Fractional Variability	21.9%
Hardness ₄₅	16.0%
Hardness ₂₃	15.8%
Spectral Index	13.0%
Hardness ₁₂	12.7%
Hardness ₃₄	11.8%
Curvature	8.8%

Note. — List of the training variables for the Classification Tree: each variable is ranked according to its relevance in the discrimination process, as computed by the CT algorithm.

Table 4. Summary of γ -ray properties and classification results

IFGL Name	R.A. (J2000)	Dec. (J2000)	l	b	Var ^a BSL ^b	Class Tree Predict Class	Logistic Reg. Predict Class	Combined Class	Radio Imaging	Radio Timing	X-Ray TeV
J0000.8+6600c	0.209	66.002	117.812	3.635		0.64	0.08				
J0001.9–4158	0.483	–41.982	334.023	–72.029		0.84	0.00	AGN	T		
J0003.1+6227	0.798	62.459	117.388	0.108		0.77	0.06	AGN	T		
J0004.3+2207	1.081	22.123	108.757	–39.448		0.87	0.00	AGN	T		
J0005.1+6829	1.283	68.488	118.689	5.999		0.78	0.00	AGN			
J0006.9+4652	1.746	46.882	115.082	–15.311		0.87	0.00	AGN	T		
J0008.3+1452	2.084	14.882	107.655	–46.708		0.77	0.00	AGN			
J0009.1+5031	2.289	50.520	116.089	–11.789		0.85	0.00	AGN			
J0016.6+1706	4.154	17.108	111.135	–44.964		0.87	0.00	AGN			
J0017.7–0019	4.429	–0.326	104.735	–62.001		0.84	0.00	AGN			

Note. — Summary of the γ -ray properties of the IFGL unassociated sources. The table includes flags for variability, predictor values for both Classification Tree and Logistic Regression analyses, combined classification, and flags indicating what type of follow-up observations are recommended. **This table is published in its entirety in the electronic edition of the *Astrophysical Journal*. A portion is shown here for guidance regarding its form and content.**

^aT indicates the source was found to be variable in the IFGL catalog analysis (Abdo et al. 2010a).

^bT indicates the source was reported in the *Fermi*-LAT Bright Source List (Abdo et al. 2009f).

Table 5. List of the predictor variables for the LR model.

Variable	Coefficient	Standard Error	p-value
Intercept	-22.17	4.97	<0.001
Fractional Variability	10.61	1.49	<0.001
Spectral Index	11.30	2.47	<0.001
Hardness ₂₃	-3.84	1.27	0.002
Hardness ₃₄	8.14	1.53	<0.001
Hardness ₄₅	3.72	0.76	<0.001
Hardness ₁₂	0.242
glat	0.333
glon	0.144

Note. — Variables selected for the Logistic Regression analysis are listed at top. Those rejected are listed below the line.

Table 6. Comparison of results for the classification techniques

	Classification		
	AGN	Pulsar	Unclassified
CT Totals	304	160	166
For $ b > 10^\circ$	244	33	96
For $ b < 10^\circ$	60	127	70
LR Totals	368	122	140
For $ b > 10^\circ$	276	39	58
For $ b < 10^\circ$	92	83	82
Combined	386	177	53
For $ b > 10^\circ$	300	50	22
For $ b < 10^\circ$	86	127	31
	LR Class		
CT Class	AGN	Pulsar	Unclassified
AGN	269	<i>2</i>	33
Pulsar	<i>32</i>	72	56
Unclassified	94	31	41

Note. — Summaries for both high and low-Galactic latitude classification results for the Logistic Regression (LR) and Classification Tree (CT) techniques, as well as for the combined sample of classified sources (14 sources with conflicting classification are not included). In addition an inter-comparison of the two classification techniques is provided. Italics indicate conflicting results, while bold indicates agreement. All 630 1FGL sources are represented here.

Table 7. Summary of follow-up observations and association efforts

IFGL Name	R.A. (J2000)	Dec. (J2000)	l	b	EGRET ^a Name	Association Identifier	Class	Observation	New ^b Observation	Figure of ^c Detections ^d Reference Merit
J0000.8+6600c	0.209	66.002	117.812	3.635
J0001.9-4158	0.483	-41.982	334.023	-72.029
J0003.1+6227	0.798	62.459	117.388	0.108	ROSAT 15
J0004.3+2207	1.081	22.123	108.757	-39.448
J0005.1+6829	1.283	68.488	118.689	5.999	...	GB6 J0008+6837	AGN	VLA	0.804	ROSAT 15
J0006.9+4652	1.746	46.882	115.082	-15.311	ROSAT 15
J0008.3+1452	2.084	14.882	107.655	-46.708	...	RX J0008.0+1450	AGN	VLA	0.700	3
J0009.1+5031	2.289	50.520	116.089	-11.789	...	NVSS J000922+503028	AGN	VLA	0.941	...
J0016.6+1706	4.154	17.108	111.135	-44.964	...	GB6 J0015+1700	FSRQ	3
J0017.7-0019	4.429	-0.326	104.735	-62.001	...	S3 0013-00	FSRQ	VLA	0.570	3

Note. — Details of the follow-up observations used to determine the new associations. Where possible, a ‘figure of merit’ was calculated for new AGN associations. Also listed are detections in other waveband that did not lead to new associations. References are given for associations based on other publications. **This table is published in its entirety in the electronic edition of the Astrophysical Journal. A portion is shown here for guidance regarding its form and content.**

^aDesignator for an EGRET source that is positionally associated.

^bIndicates what (if any) additional data was considered in determining the new association.

^cA figure-of-merit (FOM) value for sources that were associated using the technique defined in the ILAC paper (Abdo et al. 2010k); an ellipsis indicates an affiliation, which does not have enough information to calculate a FOM.

^dWaveband or catalog with association candidates.

References. — (1) Abdo et al. (2010c); (2) Abdo et al. (2010e); (3) Abdo et al. (2010k); (4) Abdo et al. (2011a); (5) Aharonian et al. (2006); (6) Aharonian et al. (2008); (7) Bird et al. (2010); (8) Castro & Slane (2010); (9) Cusumano et al. (2010); (10) Ghirlanda et al. (2010); (11) Mahony et al. (2010); (12) Mirabal (2009); (13) Mirabal et al. (2010); (14) Stephen et al. (2010); (15) Voges et al. (1994, 1999, 2000a,b); (16) Watson et al. (2008)

Table 8. Candidate VHE counterparts

1FGL Name	VHE Source Name	VHE Association	Reference
J0648.8+1516	VER J0648+152	unidentified	Ong et al. (2010)
J1503.4–5805	HESS J1503–582	unidentified	Renaud et al. (2008); Tibolla et al. (2009)
J1614.7–5138c	HESS J1614–518	<i>Pismis 22</i>	Aharonian et al. (2006)
J1702.4–4147	HESS J1702–402	PWN of PSR J1702–4128	Aharonian et al. (2008)
J1707.9–4110c	HESS J1708–410	unidentified	Aharonian et al. (2006, 2008)
J1839.1–0543	HESS J1841–055	multiple sources	Aharonian et al. (2008)
J1837.5–0659c	HESS J1837–069	unidentified	Aharonian et al. (2006)
J1844.3–0309	HESS J1843–033	unidentified	Hoppe (2008)
J1848.1–0145c	HESS J1848–018	<i>W43</i>	Tibolla et al. (2009)

Note. — Candidate VHE counterparts and their associations. Uncertain associations are in italics.

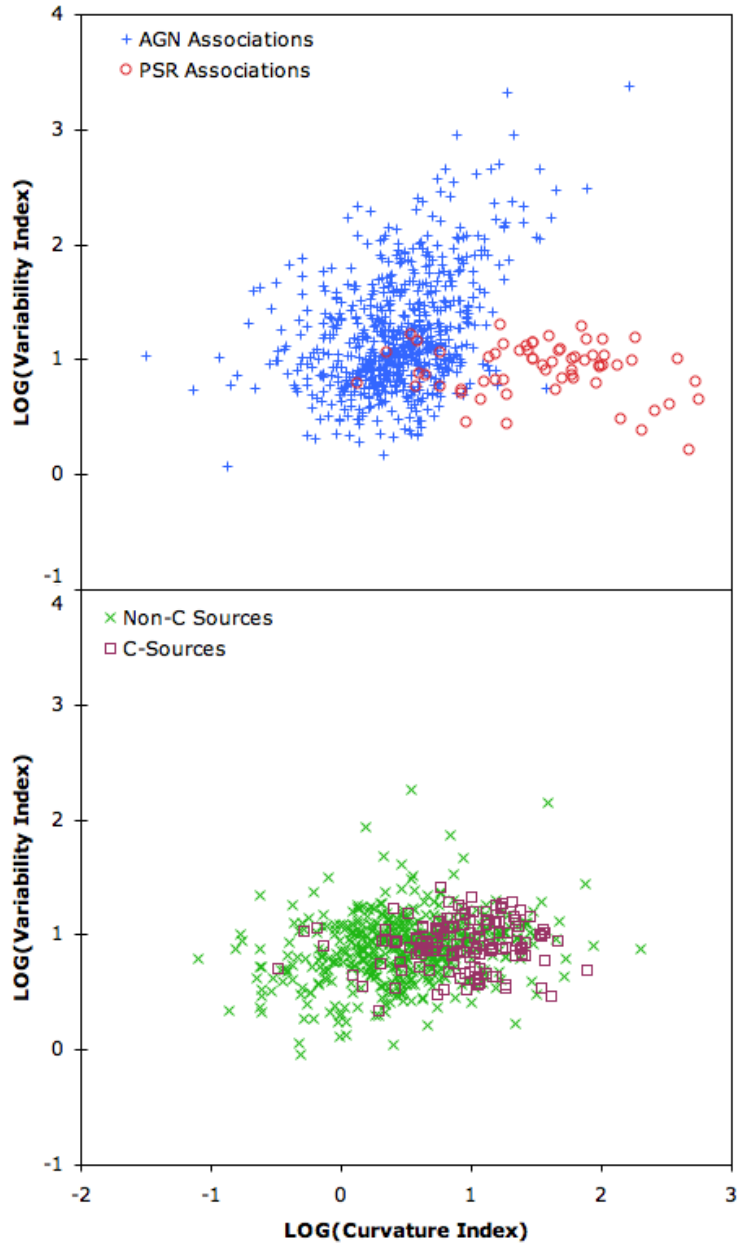


Fig. 1.— Comparison of the 1FGL Variability Index versus Curvature Index for the associated sources (top panel) and unassociated sources (bottom). A separation between the AGN (crosses) and pulsar (circles) populations is evident. However the unassociated sources mainly lie in the region where those two populations overlap.

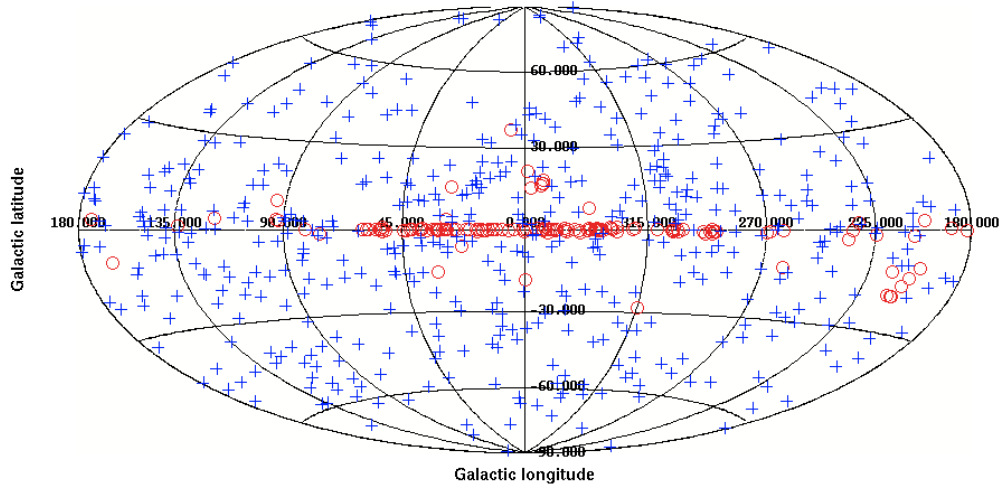


Fig. 2.— 1FGL sky map with the positions of the unassociated sources marked. Here, the non-c unassociated sources are indicated by crosses, the c-sources by circles.

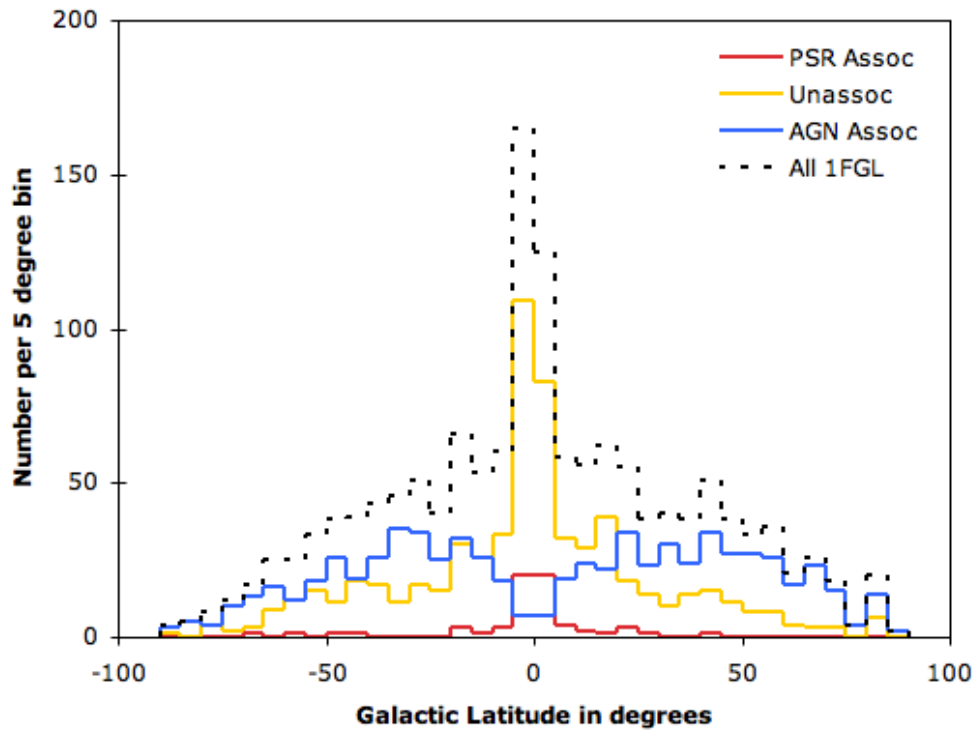


Fig. 3.— Distribution of 1FGL sources types by Galactic latitude. The sources associated with AGN (blue line) show a clear deficit at low latitudes, while the same region hosts a large number of unassociated sources (yellow line) and identified pulsars (red line).

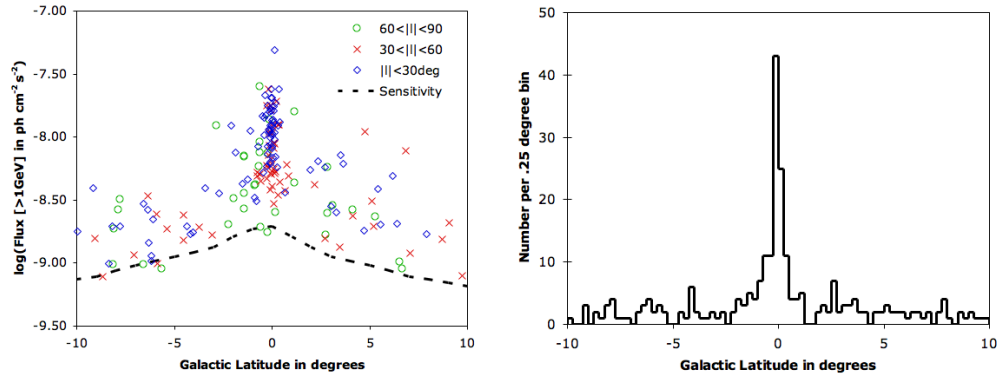


Fig. 4.— Distribution of unassociated sources in the Galactic ridge. Left: Source flux ($E > 1$ GeV) for all 1FGL sources as a function of Galactic latitude in three longitude bands. The dashed line shows the threshold flux for detectability of a source with a power-law spectrum of photon spectral index $\Gamma = 2.2$ (from the 1FGL sensitivity map, at $|l| = 0$). An increase in minimum flux is clearly visible for sources near $|b| = 0^\circ$. Right: Unassociated source counts in $0^\circ.25$ bins. A sharp peak in the number of unassociated sources is visible clustered along the central $0^\circ.5$ of Galactic latitude.

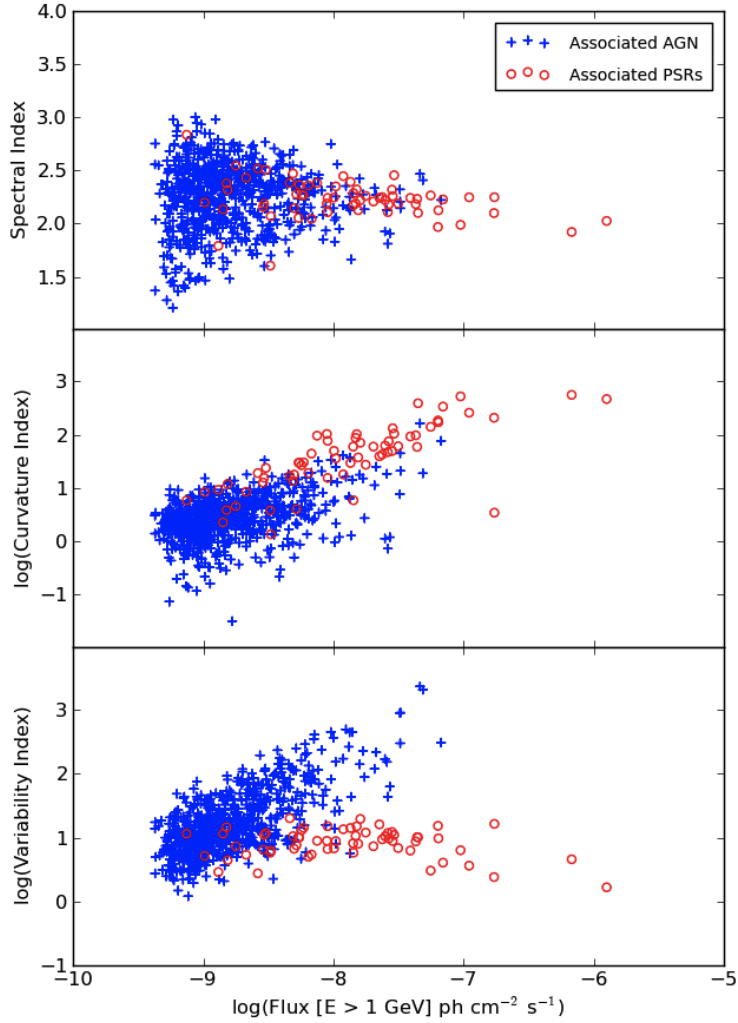


Fig. 5.— Distributions with respect to flux of the spectral index (top), curvature index (middle) and variability index (bottom) for the 1FGL associated and identified sources. It is clear that the curvature index is dependent on source flux for both AGN (crosses) and Pulsar (circles) populations. The high flux pulsar with a low value for curvature index is the Crab pulsar.

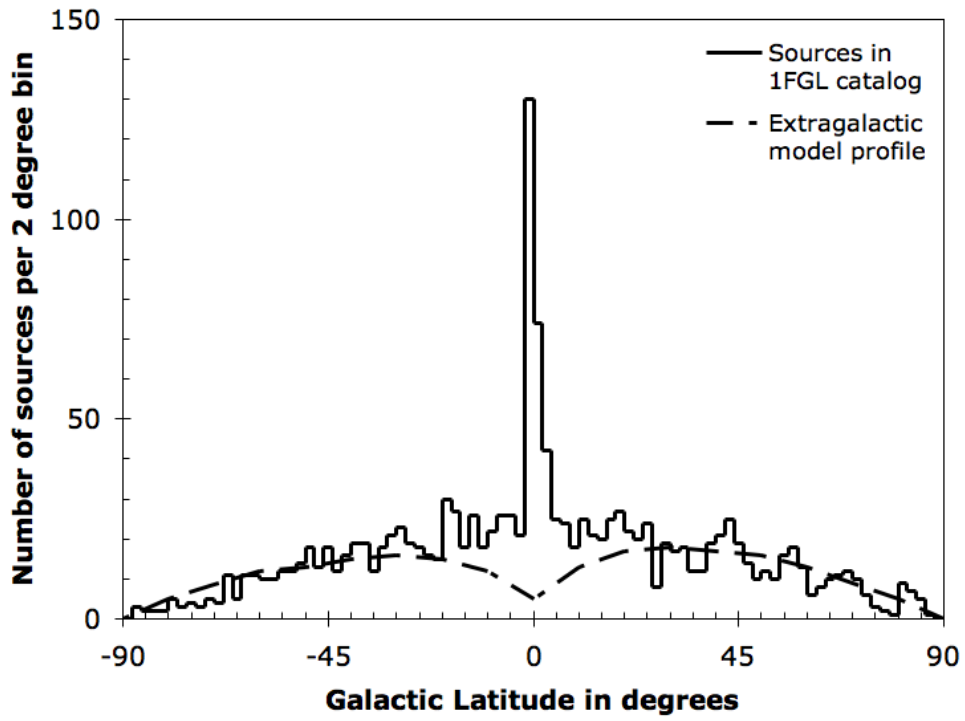


Fig. 6.— Latitude profile of the 1FGL sources and the extragalactic source model profile (dashed line)

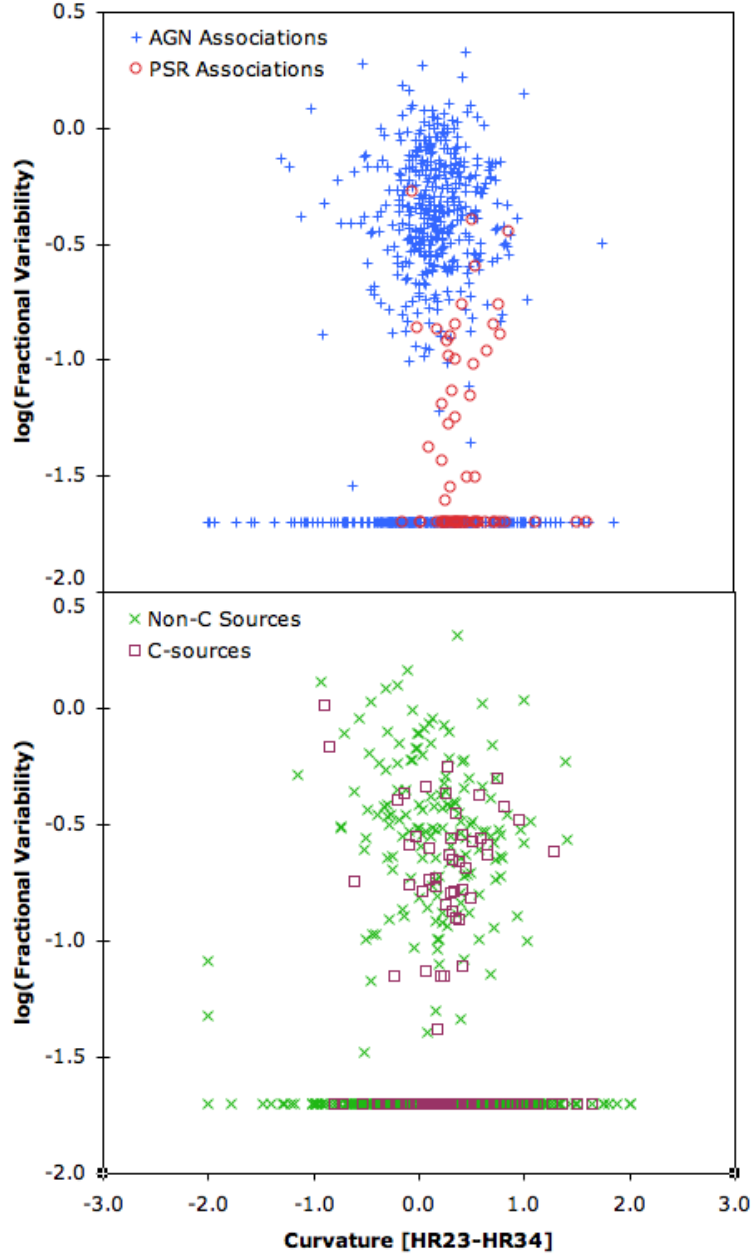


Fig. 7.— The fractional variability vs. hardness ratio difference. Top: the 1FGL associated AGN (blue crosses) and pulsars (red circles). Bottom: the 1FGL non-c unassociated sources (green crosses) and the c-sources (purple squares).

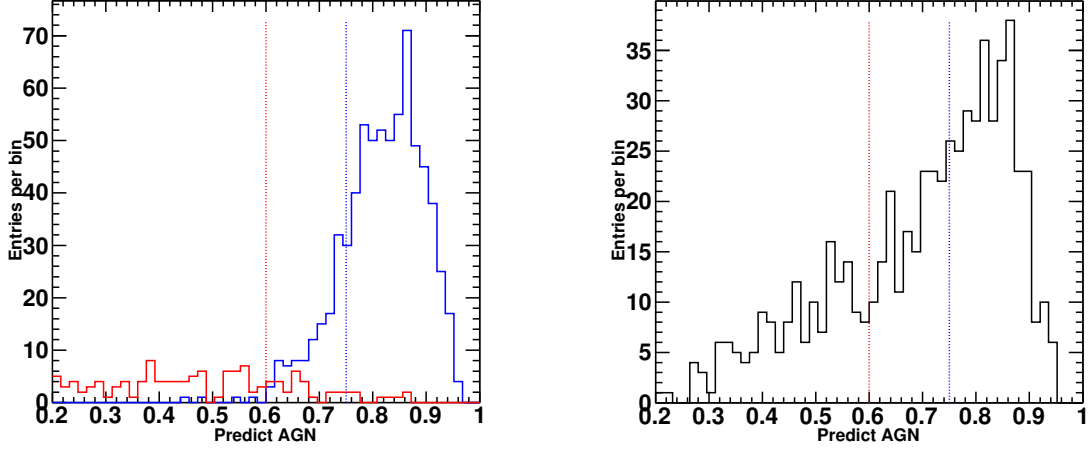


Fig. 8.— Distribution of the Classification Tree predictor. Vertical lines indicate the value of the thresholds we set to identify AGN candidates (Predictor >0.75) and pulsar candidates (Predictor <0.6). Left: sources of the 1FGL catalog identified as pulsar (red) and AGN (blue). Right: Distribution of the predictor for unassociated sources.

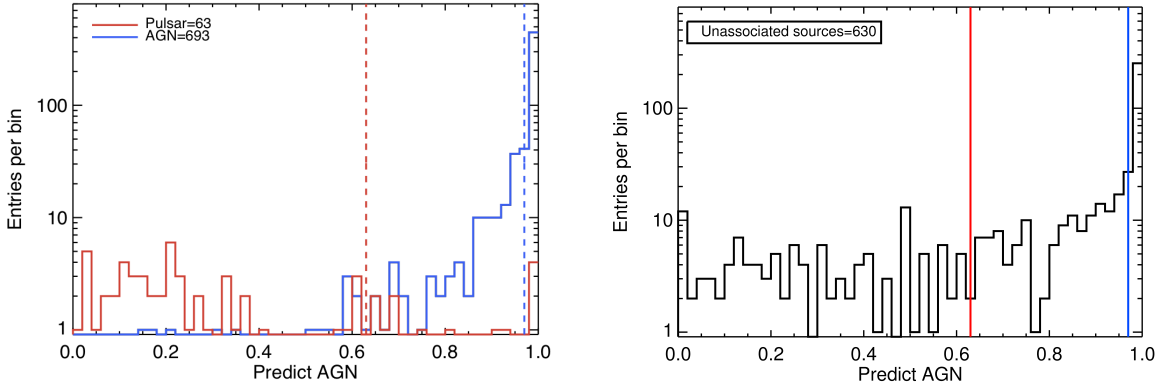


Fig. 9.— Distribution of the Logistic Regression predictor. Vertical lines indicate the value of the thresholds we set to identify pulsar candidates (Predictor <0.62) and AGN candidates (Predictor >0.98). Left: sources of the 1FGL catalog identified as pulsars (red) and AGNs (blue). Right: for 1FGL unassociated sources.

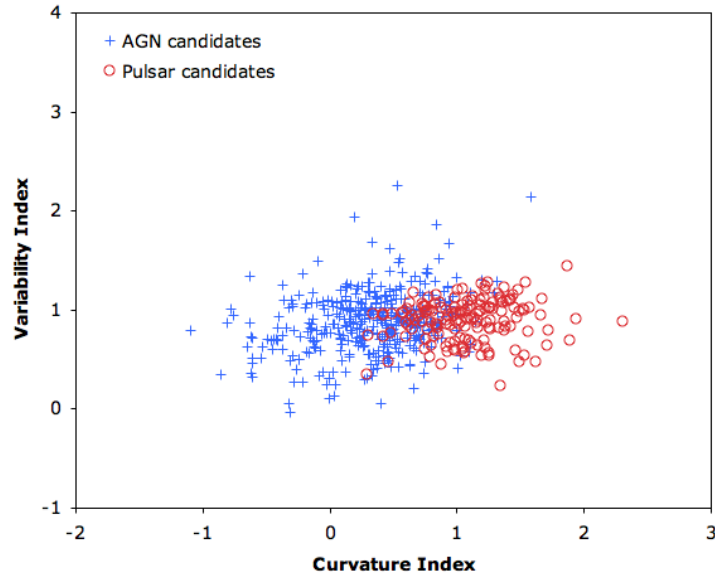


Fig. 10.— Variability index versus curvature index for 1FGL unassociated sources classified as AGN (blue crosses) and pulsar candidates (red circles).

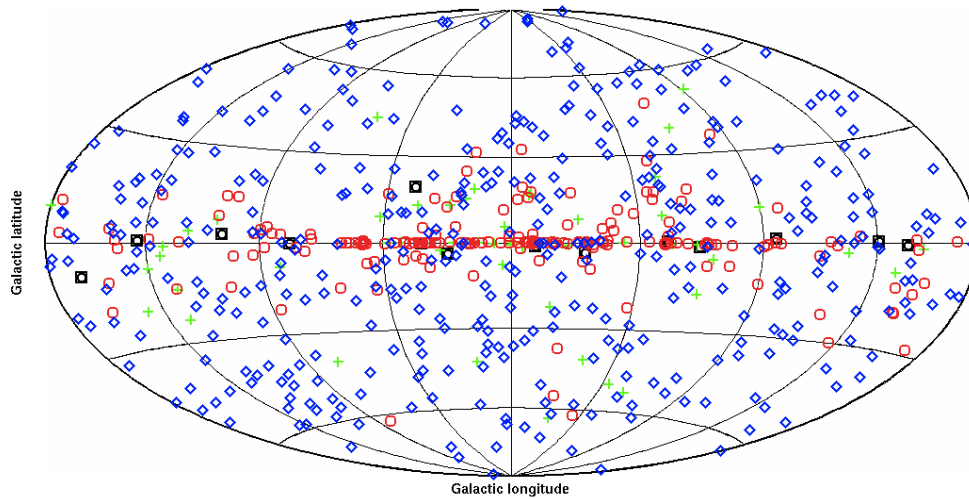


Fig. 11.— The spatial distribution of the combined classification sample, in Galactic coordinates. Sources are classified as AGN candidates (blue diamond), pulsar candidates (red circles), unclassified (green crosses), or in conflict (black squares).

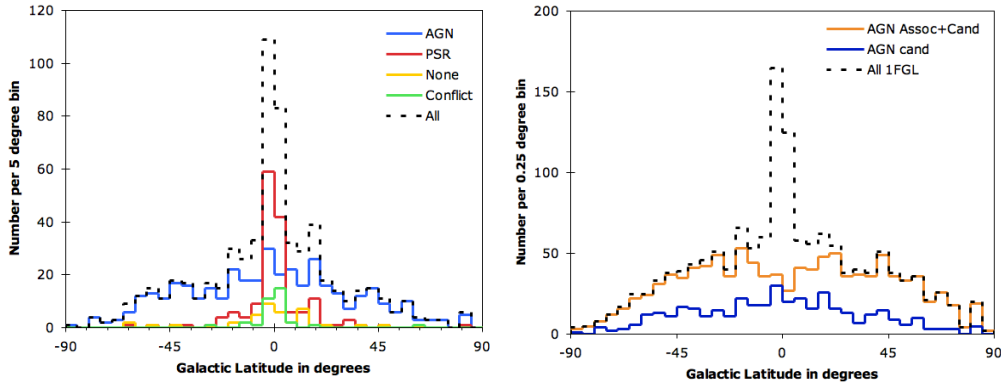


Fig. 12.— Left: Distribution of classified sources binned by Galactic latitude, with AGN in blue, pulsars in red, unclassified sources in green and sources with conflicting classification in yellow. The dashed line is the total distribution. Right: Distribution of AGN candidate binned by Galactic latitude. The orange line is the sum of the 1FGL AGN associations plus the sources classified as AGN candidates (blue line). The dashed line is the distribution for all 1FGL sources.

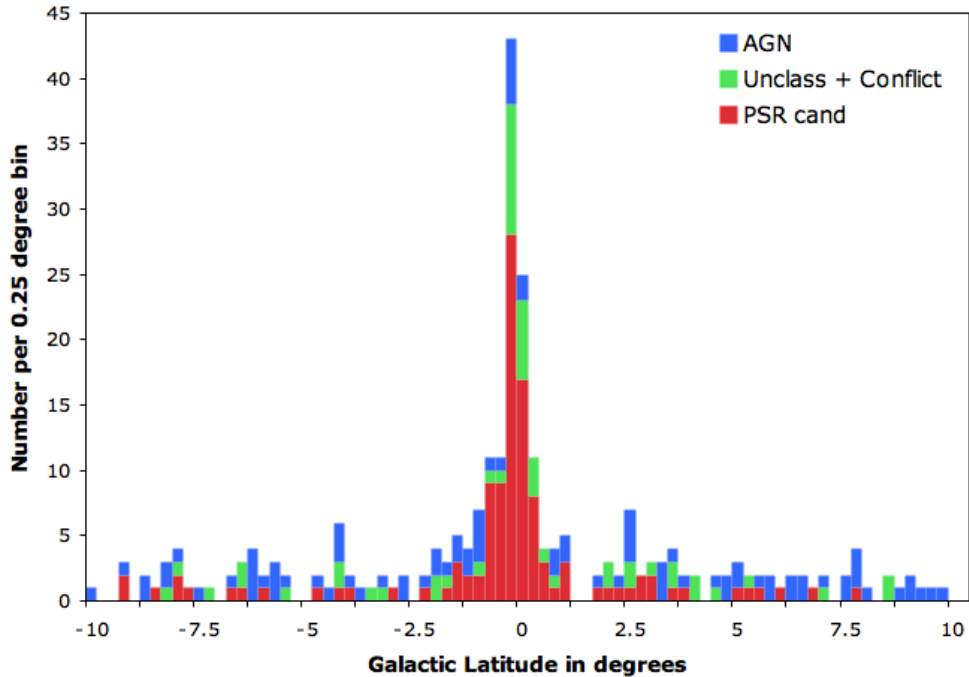


Fig. 13.— The 1FGL unassociated sources in the central few degrees of the Galaxy can be mostly separated into those classified as pulsars (red) and those that have conflicting classifications or were unable to be classified (green). The few remaining sources were classified as AGN (blue).